EMBRY-RIDDLE
Aeronautical University
DAYTONA BEACH, FLORIDA

Department of Aerospace Engineering
AE 506 Airplane Dynamic Stability

Students: Nicholas Hillburn
Anupama Kar
Edison Martinez
Dinakar Ramagalla

Professor: Dr. Richard P. Anderson

April, 2025

Contents

List of Figures . . . 3
List of Tables . . . 5
List of Abbreviations . . . 6

I Handling Qualities 8

1 Simulation 9
1.1 Trim Algorithm . . . 9
1.2 Hardware-in-the-Loop Integration and OTW View . . . 10
1.3 Trim Verification Results . . . 11
1.4 Simulink Aircraft Modeling Architecture . . . 12

II Piloted Control Systems 14

2 Fly-by-wire 15
2.1 Overview of the p-β Controller . . . 15
2.2 Controller Structure and Dynamics . . . 16
2.3 Block Diagram Implementation . . . 16
2.4 Simulation Results . . . 18

III Autonomous Control Systems 21

3 Longitudinal Control Tasks 22
3.1 Stage 1 - Climb . . . 23
3.1.1 Part 1 - Achieving an 80° Flight Path Angle . . . 23
3.1.2 Part 2 – Maintaining the Flight Path Angle . . . 24
3.2 Stage 2 - Pitch Maneuver . . . 26
3.3 Stage 3 – Reentry Phase . . . 28
3.3.1 Part 1 – Controlled Reentry Pitch Angle . . . 28
3.3.2 Part 2 - Reentry . . . 28
3.4 Flight Overview . . . 30

4 Lateral-Directional Control Tasks 32
4.1 Incremental Nonlinear Dynamic Inversion (INDI) . . . 33
4.2 Stage 4 – Heading Reversal 180° . . . 34
4.3 Stage 5 - Waypoint Tracking . . . 35
4.4 Flight Overview . . . 37

IV Modeling and Validation **39**

5 Introduction **40**
5.1 Aircraft Geometry . . . 40
5.2 Powerplant and Propeller . . . 41
5.3 Reference Datum . . . 42
5.4 Instrumentation Locations . . . 42
5.5 Weight and Balance . . . 42
5.5.1 Weight and Balance Log Entries . . . 47
5.6 Aerodynamic Center Location and Mean Aerodynamic Chord . . . 48
5.7 Thrust Application Point . . . 50
5.8 Diamond DA42 Aircraft . . . 51

6 Longitudinal Modeling **53**
6.1 Engine and Propeller Model . . . 53
6.1.1 Lookup Table Construction . . . 54
6.1.2 Propeller Efficiency . . . 54
6.2 Simulation Setup . . . 54
6.3 Aerodynamic Modeling . . . 55
6.3.1 Procedure Using SIDPAC . . . 56
6.3.2 Automation and Model Formulation . . . 56
6.3.3 Integration into Simulink . . . 57
6.4 Drag Curve Tuning . . . 59
6.4.1 Trim Segment Selection and Reference Generation . . . 59
6.4.2 Iterative Correction of C_D . . . 59
6.4.3 Final Drag Curve . . . 60

7 Lateral-Directional Modeling **63**
7.1 Bias Correction . . . 63

8 Static Derivatives **64**
8.1 Drag coefficient approximation . . . 64
8.2 Lift coefficient approximation . . . 65
8.3 Pitching moment coefficient approximation . . . 66

9 Validation **68**
9.1 Final Modifications . . . 72

A Extra Credit - Anupama Kar **75**

B Extra Credit - Edison Martinez **76**

List of Figures

1.1 Simulink model connected to flight sim controls. From the top, the Joystick controls the ailerons and elevators, the Pedals control the rudder, and the Thrust Joystick controls the power. . . . 10
1.2 Out-the-window view using FlightGear connected to Simulink. . . . 11
1.3 Attitude, altitude, and airspeed plots of the trim algorithm test by a test pilot at EFRC. The altitude is in feet, the attitude is in degrees, and the airspeed is in knots. . . . 11
1.4 Reference frames flowchart. . . . 12
1.5 Flowchart of the basics of flight sim modeling. . . . 12
1.6 Internal structure of Aircraft_Dynamics Block on Simulink model. . . . 13

2.1 Reference block diagram for lateral-directional p-β control law [1]. . . . 17
2.2 Feedback structure within the p-β control law[1]. . . . 17
2.3 ERAU implementation of the p-β controller in Simulink. Red: Reference model, Blue: Feedback, Green: Feed-Forward. . . . 18
2.4 Test 1: Pilot in the loop - Roll rate p (left) and sideslip β (right). . . . 18
2.5 Test 2: Pilot + turbulence - Effects of external disturbance on control. . . . 19
2.6 Turbulence signal for Test 2. . . . 19
2.7 Test 3: Turbulence only - roll and sideslip response without pilot input. . . . 20
2.8 Turbulence signal for Test 3. . . . 20

3.1 Top-level Simulink model of the spacecraft controller. . . . 22
3.2 Simulink model: Stage 1 (Below 5,000 ft altitude). . . . 23
3.3 Climb phase results: Reaching 80° FPA. . . . 24
3.4 Simulink model: Stage 2 (Below 124,000 ft altitude). . . . 25
3.5 Climb phase results: Maintaining FPA. . . . 25
3.6 Complete climb profile with FPA regulation and g-load envelope. . . . 26
3.7 Simulink model: Stage 3 (Pitch maneuver control). . . . 27
3.8 Pitch maneuver execution between 130–330 seconds. . . . 27
3.9 Simulink model: Stage 4 (Controlled reentry pitch). . . . 28
3.10 Simulink model: Stage 5 (Final reentry phase). . . . 29
3.11 Reentry profile with pitch modulation to minimize g-load and thermal stress. . . . 29
3.12 Altitude profile showing ascent to 600,000 ft and descent. . . . 30
3.13 Full flight simulation results. . . . 31

4.1 Top-level lateral-directional control architecture in Simulink. . . . 32
4.2 Euler angle command generation block. . . . 33
4.3 INDI implementation in Simulink for lateral-directional control. . . . 34
4.4 Euler command logic for heading reversal maneuver. . . . 34
4.5 Euler angle tracking during 180° heading reversal. . . . 35
4.6 Euler command logic for waypoint navigation. . . . 36
4.7 Euler angle tracking while navigating to the waypoint. . . . 36
4.8 Complete flight profile: commanded vs. actual Euler angles. . . . 37

4.9 Trajectory plot showing successful approach to the waypoint. 38

5.1 Cessna 182Q Aircraft 40
5.2 Loading Arrangements 46
5.3 Cabin height and width measurements 47
5.4 The location of 25% $\bar{c}$ with respect to the datum (39.18 inches) - Side view . . . 49
5.5 The location of 25% $\bar{c}$ with respect to the datum (39.18 inches) - Top view . . . 50
5.6 Diagram showing the thrust application point on the Cessna 182Q. 51

6.1 Engine and propeller integration flowchart. 53
6.2 Simulink model of the engine. 54
6.3 Drag coefficient C_D as a function of angle of attack α. 57
6.4 Lift coefficient C_L as a function of angle of attack α. 58
6.5 Pitching moment coefficient C_m as a function of angle of attack α. 58
6.6 MAP comparison between raw flight data, smoothed flight data and simulation (no drag correction). 59
6.7 MAP comparison between raw flight data, smoothed flight data and simulation (MAP matching). 60
6.8 Comparison of original and corrected drag curves. 61
6.9 Final blended drag curve used in simulation. 61
6.10 MAP comparison between raw flight data, smoothed flight data and simulation (corrected drag curve). 62

8.1 Comparison of C_D from flight data, regression model, and approximation as a function of angle of attack. 65
8.2 Comparison of C_L from flight data, regression model, and approximation as a function of angle of attack. 66
8.3 Comparison of C_m from regression model and approximation as a function of angle of attack. 67

9.1 Validation result for angle of attack (α). 69
9.2 Validation result for vertical acceleration (N_z). 69
9.3 Validation result for pitch rate (q). 70
9.4 Validation result for sideslip angle (β). 71
9.5 Validation result for roll rate (p). 71
9.6 Validation result for yaw rate (r). 72

A.1 Function for each derivative vs. α 75

B.1 Linear fit of lift coefficient C_L vs. angle of attack α. 76
B.2 Linear fit of pitching moment coefficient C_m vs. angle of attack α. 77
B.3 Quadratic fit of drag coefficient C_D vs. angle of attack α. 78
B.4 Fitted and average comparison of elevator control derivative $C_{m_{\delta e}}$. 79
B.5 Fitted and average comparison of pitch damping derivative C_{mq}. 80

List of Tables

2.1 Navion Lateral Modes of Motion 15

5.1 Cessna 182Q Aircraft Geometry 41
5.2 Control Surface Deflections for Cessna 182Q 41
5.3 Positions of Air Data Instruments and IMU 42
5.4 Sample Airplane Weighing 44
5.5 Weight and Balance Entries 47
5.6 Basic Aircraft Weight and Balance 48
5.7 Diamond DA42 Aircraft Geometry 52
5.8 Control Surface Deflections for Diamond DA42 52

6.1 Average Values for Longitudinal Stability Derivatives 57

7.1 Average Values for Lateral-Directional Stability and Control Derivatives 63

9.1 Model Output Tolerances 68
9.2 Longitudinal Model: Control Input Biases and Time Within Tolerance 70
9.3 Lateral Model: Control Input Biases and Time Within Tolerance 72

B.1 Error Metrics for Quadratic and Average Fits 78

List of Abbreviations

Abbreviation	Full Form
α	Angle of Attack
β	Sideslip Angle
γ	Flight Path Angle
ϕ	Euler Angle (Bank)
θ	Euler Angle (Pitch)
ψ	Euler Angle (Heading)
p	Bank Rate
q	Pitch Rate
r	Yaw Rate
δ_e	Elevator Deflection
δ_r	Rudder Deflection
δ_a	Aileron Deflection
AC	Aerodynamic Center
BHP or bhp	Brake Horsepower
C_D	Coefficient of Drag
CG	Center of Gravity
C_L	Coefficient of Lift
C_l	Coefficient of Rolling Moment
$C_{L\beta}$	Dihedral Effect
C_{lp}	Roll Damping
$C_{l\delta r}$	Rudder Effect on Roll Moment
$C_{l\delta a}$	Roll Control Power
C_M or C_m	Coefficient of Pitching Moment
C_{mq}	Pitch Rate Damping Derivative
$C_{m\delta e}$	Elevator Control Derivative
$C_{n\beta}$	Weathervane Stability
C_{nr}	Yaw Damping
C_{np}	Roll Rate Influence on Yaw Moment
$C_{n\delta r}$	Yaw Control Power
C_N or C_n	Coefficient of Yawing Moment
C_Y	Side Force Derivative w.r.t. Sideslip Angle
DCM	Directional Cosine Matrices
DOF	Degrees of Freedom
EFRC	Eagle Flight Research Center
EOM	Equations of Motion
FAA	Federal Aviation Administration
FSTDs	Flight Simulation Training Devices
hp	Pressure Altitude
IC	Initial Conditions
IMU	Inertial Measurement Unit

Abbreviation	**Full Form**
INDI	Incremental Nonlinear Dynamic Inversion
LQR	Linear Quadratic Regulator
MAC	Mean Aerodynamic Chord
MIMO	Multi Input Multi Output
NDI	Nonlinear Dynamic Inversion
NED	North East Down
NEU	North East Up
N_z	Gravitational Force in the Z Direction
OAT	Outside Air Temperature
PD	Proportional Derivative
PID	Proportional-Integral-Derivative
POH	Pilot Operating Handbook
SHP	Shaft Horsepower
TCDS	Type Certification Data Sheet

Part I

Handling Qualities

Chapter 1

Simulation

Chapter Objectives

1. **Implement Aircraft Trimming:** Automatically trim the aircraft at the start of each simulation using a trim algorithm.
2. **Integrate Pilot-in-the-Loop Controls:** Connect physical controls (joystick, pedals, and throttle) to Simulink for pilot-in-the-loop simulations.
3. **Demonstrate Out-the-Window View and Manual Flight:** Validate real-time simulation performance using an out-the-window (OTW) visualization and manual stick control.

This chapter presents the simulation environment for the Navion aircraft, emphasizing trimming, pilot control integration, and full aircraft modeling in Simulink.

1.1 Trim Algorithm

Aircraft trimming is an essential element in aviation as it allows to have an steady, hands-off flight. It minimizes control surface deflections required to maintain stable flight conditions. To implement this, the `jj_trim` algorithm was integrated into our aircraft model to calculate the necessary elevator and throttle inputs that balance aerodynamic and propulsion forces.

Initial conditions were configured for level flight at 5000 ft altitude and a forward velocity of 168.78 ft/s (100 kts). The algorithm solves the steady-state equations to ensure net accelerations and moments approach zero.

1.2 Hardware-in-the-Loop Integration and OTW View

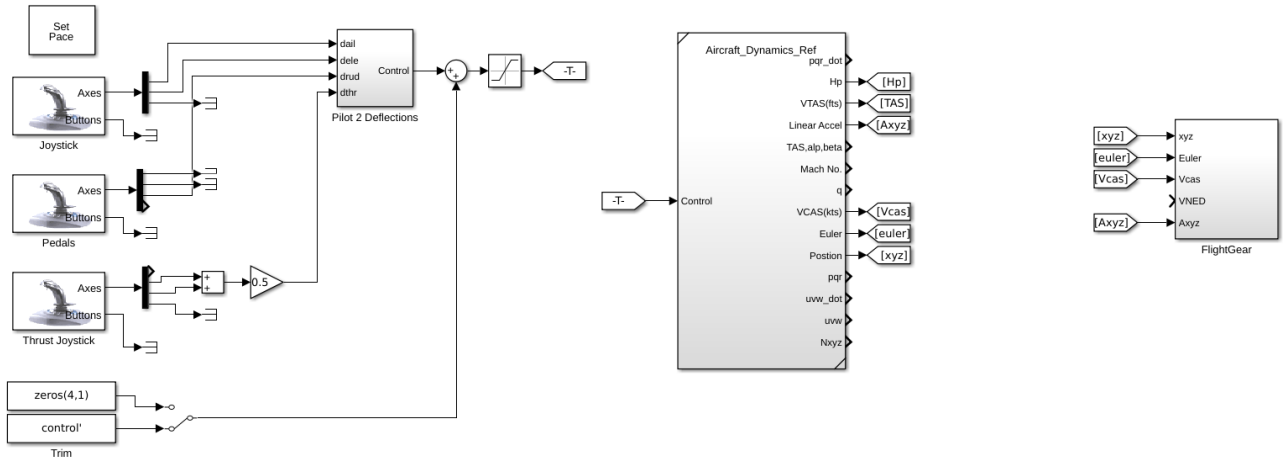

Figure 1.1: Simulink model connected to flight sim controls. From the top, the Joystick controls the ailerons and elevators, the Pedals control the rudder, and the Thrust Joystick controls the power.

The Simulink model was connected to a flight simulator setup at EFRC (Eagle Flight Research Center) to enable real-time pilot-in-the-loop testing. Control mappings were set as follows:

- **Joystick**: Aileron and elevator (bank and pitch)
- **Rudder Pedals**: Rudder (yaw)
- **Throttle Handle**: Engine thrust

Control input ranges were aligned with the Type Certificate Data Sheet (TCDS) to ensure realistic deflection limits. During these tests, an out-the-window (OTW) view was also integrated using FlightGear. The connection was made through the Simulink FlightGear interface blocks provided by MATLAB, allowing real-time visualization of the aircraft from a pilot's perspective.



Figure 1.2: Out-the-window view using FlightGear connected to Simulink.

1.3 Trim Verification Results

The test pilot verified the trim behavior with zero pilot input and observed level flight maintained at 5000 ft with a pitch angle around 0.025°. Figure 1.3 shows the validation plots for altitude, attitude, and airspeed.

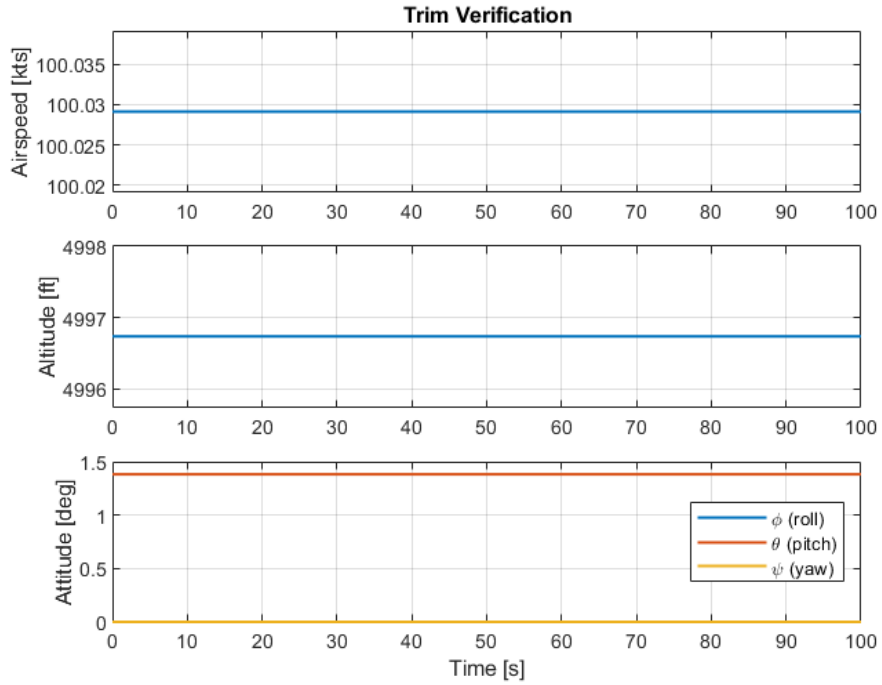

Figure 1.3: Attitude, altitude, and airspeed plots of the trim algorithm test by a test pilot at EFRC. The altitude is in feet, the attitude is in degrees, and the airspeed is in knots.

1.4 Simulink Aircraft Modeling Architecture

The simulation relies on a design split into reference frames and subsystems:

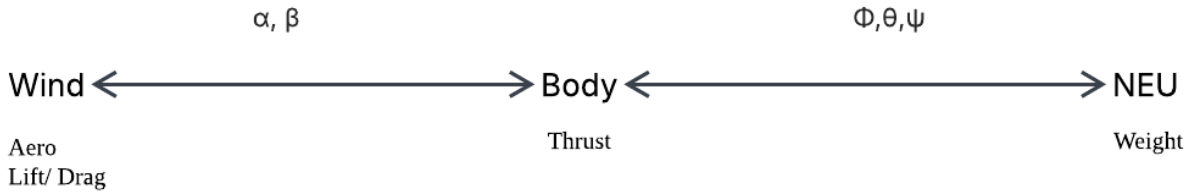

Figure 1.4: Reference frames flowchart.

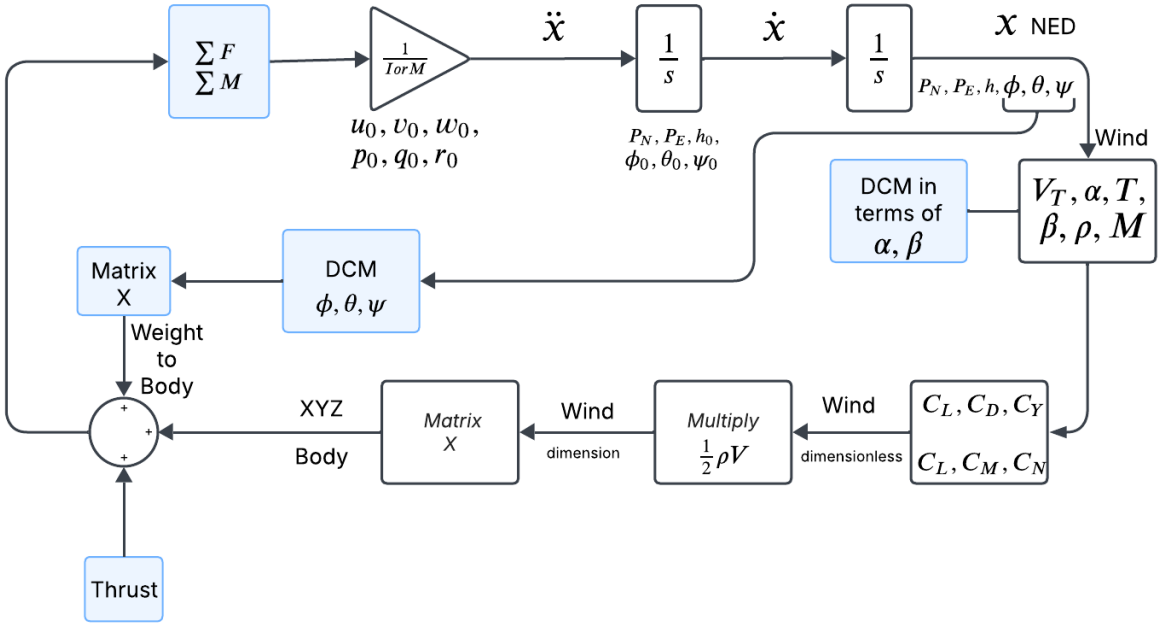

Figure 1.5: Flowchart of the basics of flight sim modeling.

This structure is implemented within the `Aircraft_Dynamics` block in Simulink (Figure 1.6).

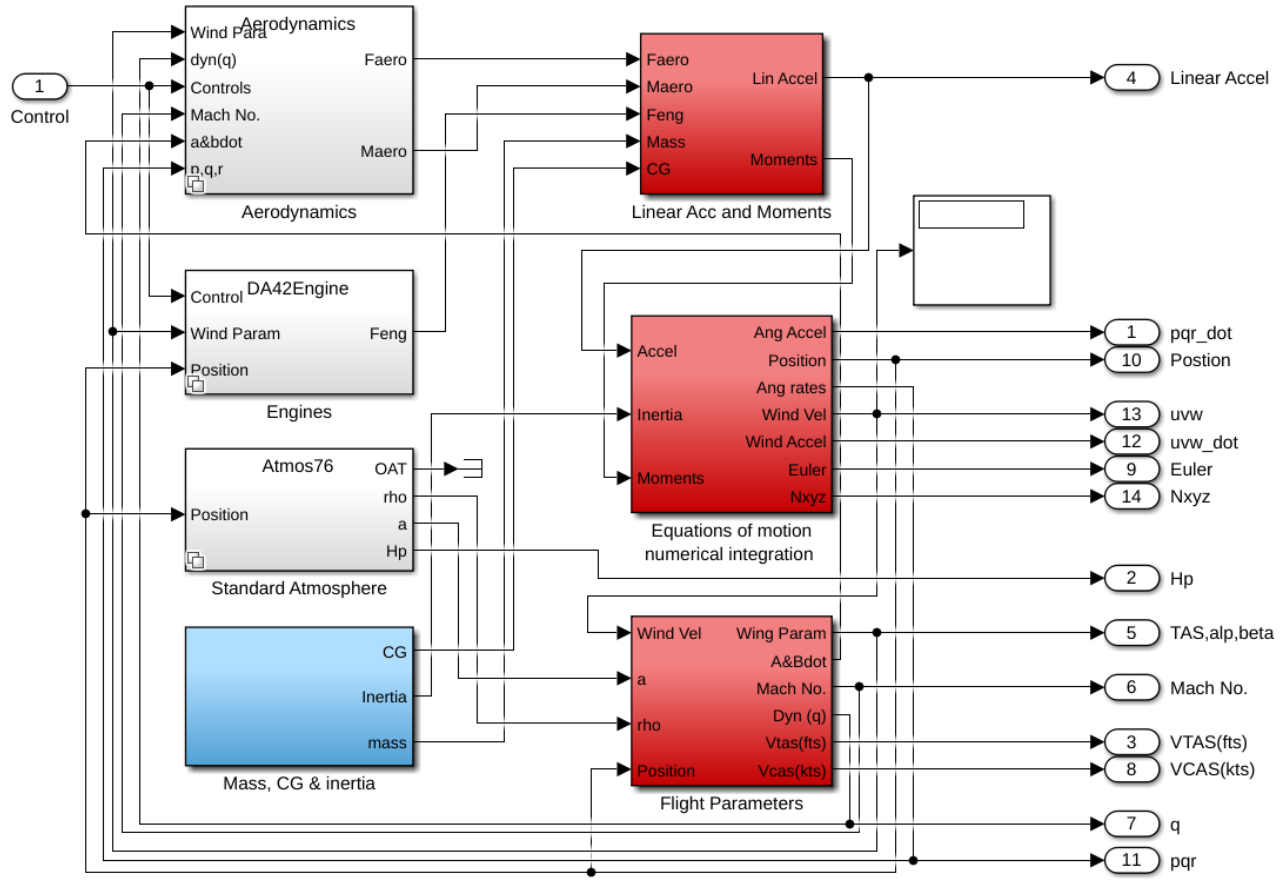

Figure 1.6: Internal structure of Aircraft_Dynamics Block on Simulink model.

The main `Aircraft_Dynamics` block contains:

- **Aerodynamics**: Computes forces/moments from control surfaces and airflow conditions.
- **Engine Model**: Converts throttle commands to thrust.
- **Standard Atmosphere**: Provides density and pressure for altitude variations.
- **Mass and Inertia**: Computes inertial effects from CG and aircraft weight.
- **Equations of Motion (EOM)**: Integrates forces/moments into velocities and Euler angles.

Part II

Piloted Control Systems

Chapter 2

Fly-by-wire

Chapter Objectives

1. **Background on p-β Control:** Understand the mathematical formulation and linearization of aircraft dynamics.
2. **Controller Implementation:** Apply the p-β controller to the Navion aircraft model in Simulink to improve lateral-directional stability.
3. **Evaluation:** Analyze simulation results under various flight conditions (with and without turbulence) to assess the performance of the controller.

2.1 Overview of the p-β Controller

The p-β controller is designed to improve lateral-directional stability, especially in fly-by-wire systems. It targets control of the roll rate p and sideslip angle β, automatically coordinating aileron and rudder inputs. This chapter follows the implementation described by Tischler and Berger et al. [1].

Aircraft dynamics are inherently nonlinear, requiring linearization for control design. Using MATLAB's Model Linearizer, the Navion model was linearized around its lateral-directional dynamics, yielding the following dominant modes:

Table 2.1: Navion Lateral Modes of Motion

Mode	**Time Constant (s)**	**Natural Frequency (rad/s)**	**Damping Ratio**
Dutch Roll	2.3546	2.1617	0.1965
Roll	0.1438	–	–
Spiral	230.6297	–	–

Two key characteristics of the p-β controller are essential for understanding its flight handling implications:

1. **Hold of Commanded Roll Rate:** Once a roll rate is commanded, the controller continues to maintain that rate until a new command is received. This means that for the aircraft to return to wings-level flight, the pilot must actively command zero roll rate; simply releasing the stick is not enough.
2. **Automatic Rudder Coordination:** The controller automatically generates rudder deflections in response to aileron inputs. This eliminates the need for manual rudder input during turns, improving turn coordination and reducing workload, especially in turbulent conditions.

2.2 Controller Structure and Dynamics

The controller includes dynamic models for both the roll rate and sideslip reference signals. The commanded dynamics are modeled as:

$$\frac{p_{\text{cmd}}}{\delta_{\text{wheel}}} = \frac{1}{\tau_{pcmd}s + 1}, \qquad \frac{\beta_{\text{cmd}}}{\delta_{\text{pedal}}} = \frac{\omega^2}{s^2 + 2\zeta\omega s + \omega^2}$$

The roll rate reference model is represented by a first-order system, where τ_{pcmd} corresponds to the time constant of the roll mode. On the other hand, the sideslip dynamics are modeled using a second-order system, reflecting the more complex and oscillatory nature of β due to its dependence on both yaw and lateral aerodynamic effects. The damping ratio is set to 0.7, and the natural frequency is matched to the Dutch roll frequency, ensuring realistic dynamic coupling and allowing the rudder to effectively dampen sideslip oscillations.

LQR optimization is used to derive the initial gain matrix K, balancing performance (via Q) and control effort (via R). Gains are then refined manually or via CONDUIT®. The controller consists of:

- **Feedforward gains:** Track commanded signals.
- **Feedback gains:** Minimize error between commanded and actual p, β.
- **Cross-feed gains:** Coordinate rudder and aileron inputs to improve performance and reduce adverse yaw.

2.3 Block Diagram Implementation

Figures 2.1 and 2.2 show the reference diagrams from the literature. Figure 2.3 shows the Simulink implementation. The top-level diagram includes the reference model (red), feedback loop (blue), and feedforward path (green).

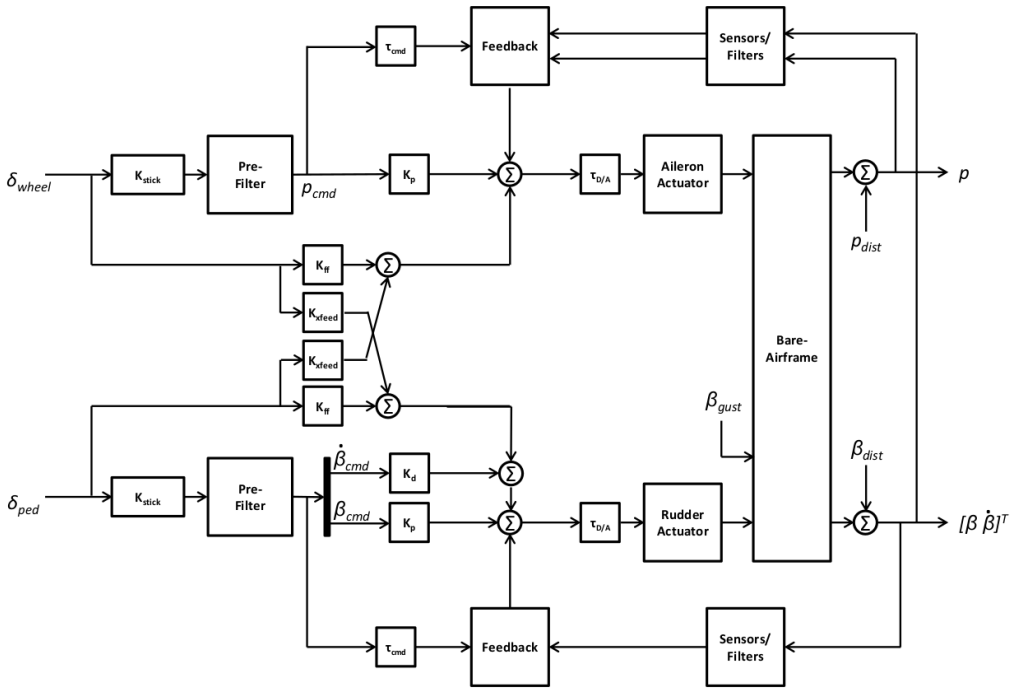

Figure 2.1: Reference block diagram for lateral-directional p-β control law [1].

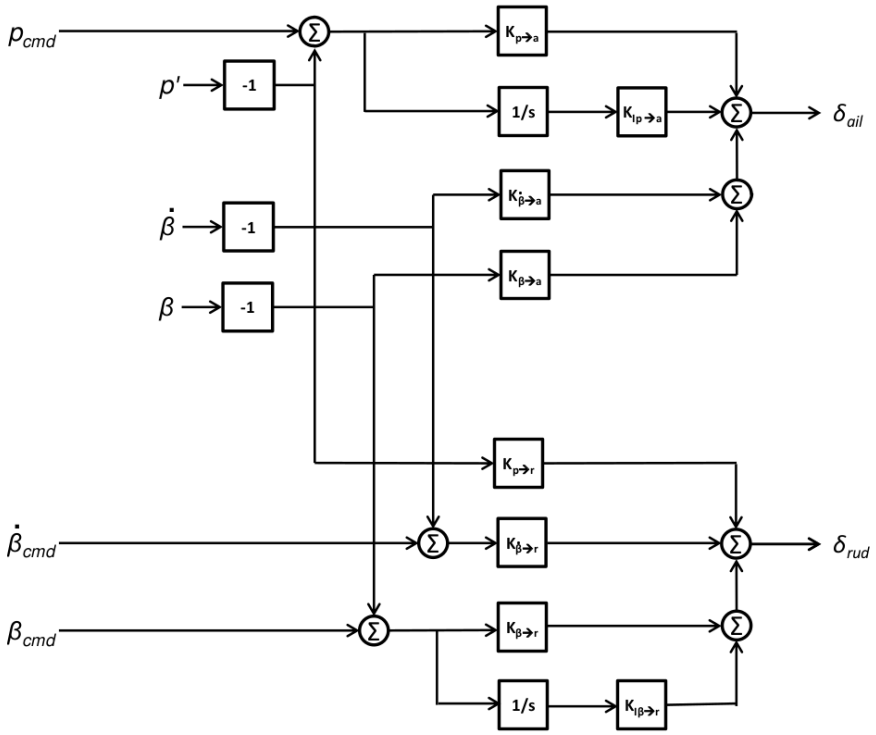

Figure 2.2: Feedback structure within the p-β control law[1].

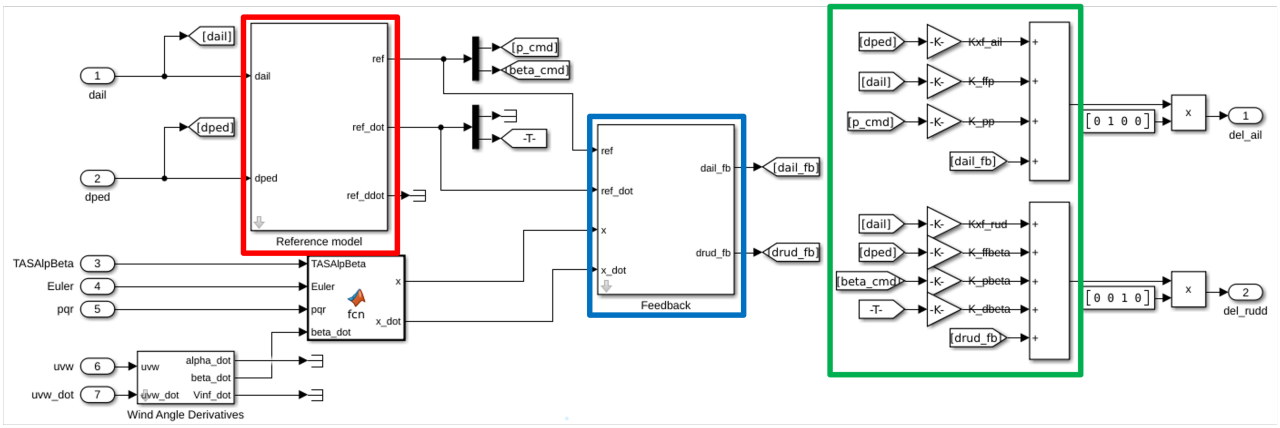

Figure 2.3: ERAU implementation of the p-β controller in Simulink. Red: Reference model, Blue: Feedback, Green: Feed-Forward.

2.4 Simulation Results

Three test conditions were evaluated:

- Pilot in the loop (no turbulence)
- Pilot in the loop with turbulence
- Turbulence only (pilot commands disabled)

In each case, the controller's objective was to track a reference signal (or maintain zero reference in the turbulence-only test) by coordinating roll rate p and sideslip β, while minimizing control effort.

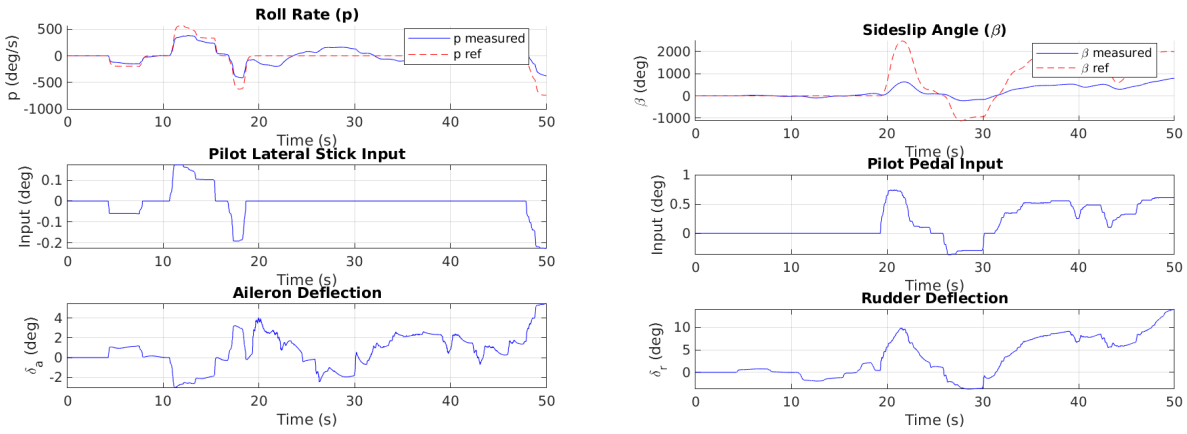

Figure 2.4: Test 1: Pilot in the loop - Roll rate p (left) and sideslip β (right).

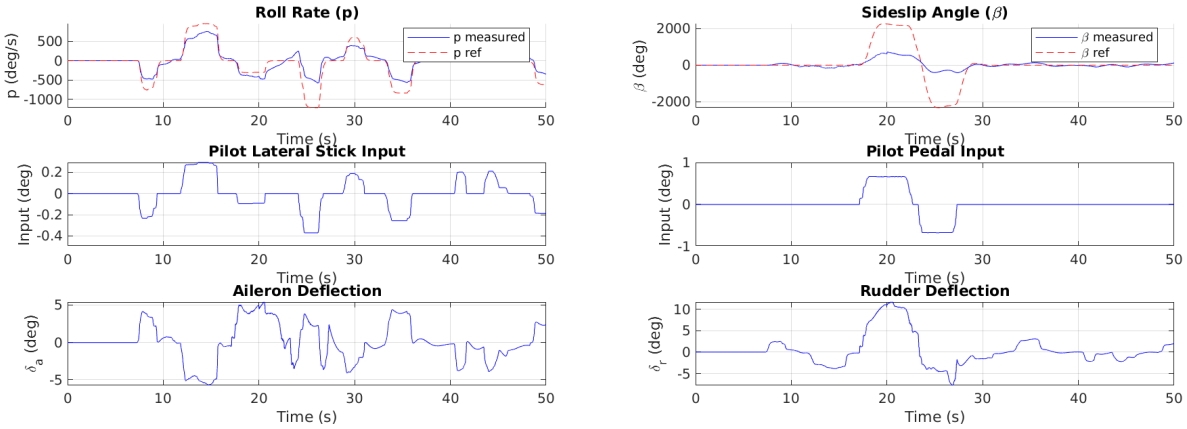

Figure 2.5: Test 2: Pilot + turbulence - Effects of external disturbance on control.

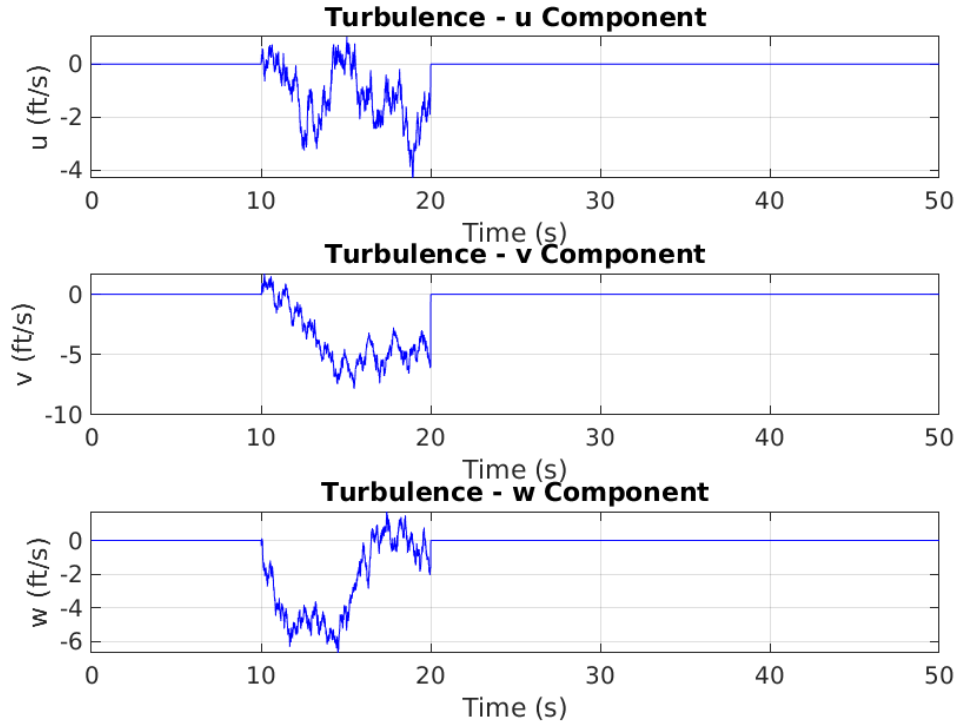

Figure 2.6: Turbulence signal for Test 2.

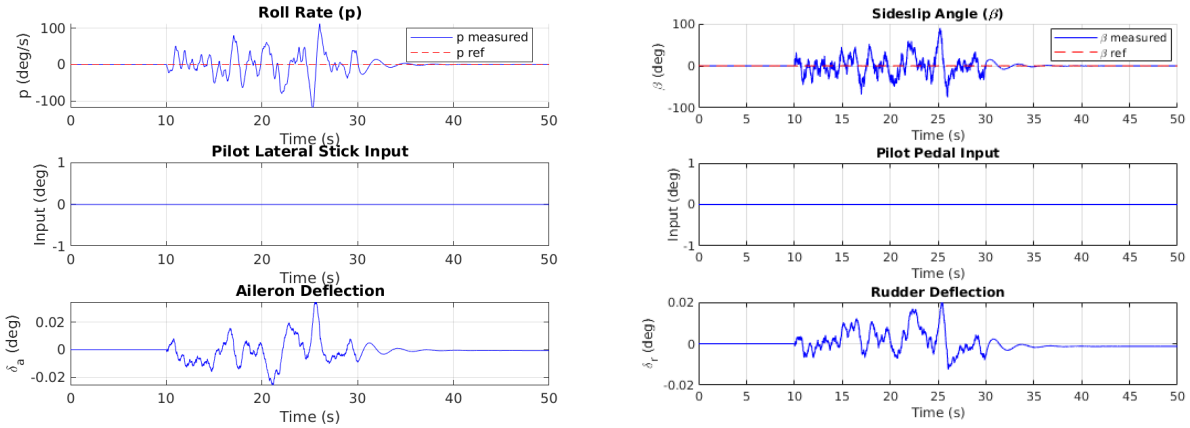

Figure 2.7: Test 3: Turbulence only - roll and sideslip response without pilot input.

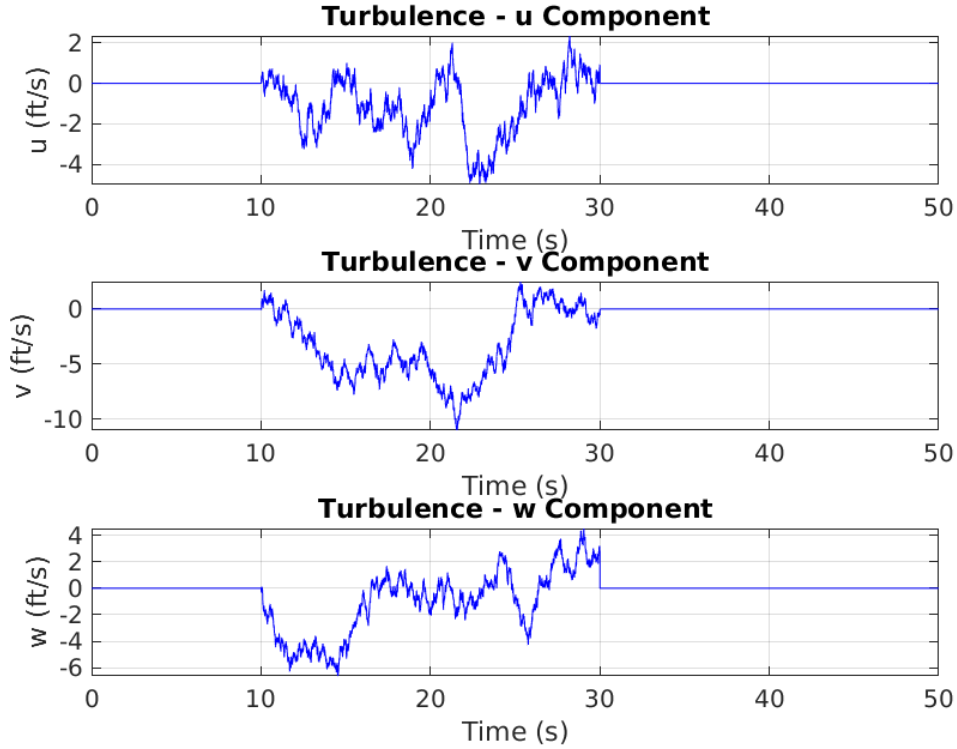

Figure 2.8: Turbulence signal for Test 3.

Part III

Autonomous Control Systems

Chapter 3

Longitudinal Control Tasks

Chapter Objectives

1. **Airborne Launch and Climb:** Simulate an airborne launch sequence. Stabilize the initial drop for two seconds before igniting the rocket engines. Transition into a controlled climb up to 40,000 ft.

2. **High-Altitude Pitch Maneuvers:** Execute a full 360° pitch maneuver in both positive and negative directions.

3. **Reentry Strategy:** Design and test a glide-based reentry strategy that minimizes thermal loading and g-forces, ensuring a safe return to Earth's surface.

This chapter presents a spacecraft dynamics simulation aimed at understanding control behavior in high-altitude and near-space environments. The simulation models the full flight of a rocket-powered vehicle, from an airborne launch to apogee at 600,000 ft, and finally through atmospheric reentry. The Earth's atmosphere becomes non-standard above approximately 50,000 ft, and thus the simulation accounts for varying atmospheric density, pressure, and temperature throughout the climb and descent.

The flight vehicle is a modified, rocket-powered Navion modeled in 6 degrees of freedom (6DoF) using Simulink. The simulation includes a custom propulsion model and a modular control architecture. The top-level Simulink model is shown in Figure 3.1.

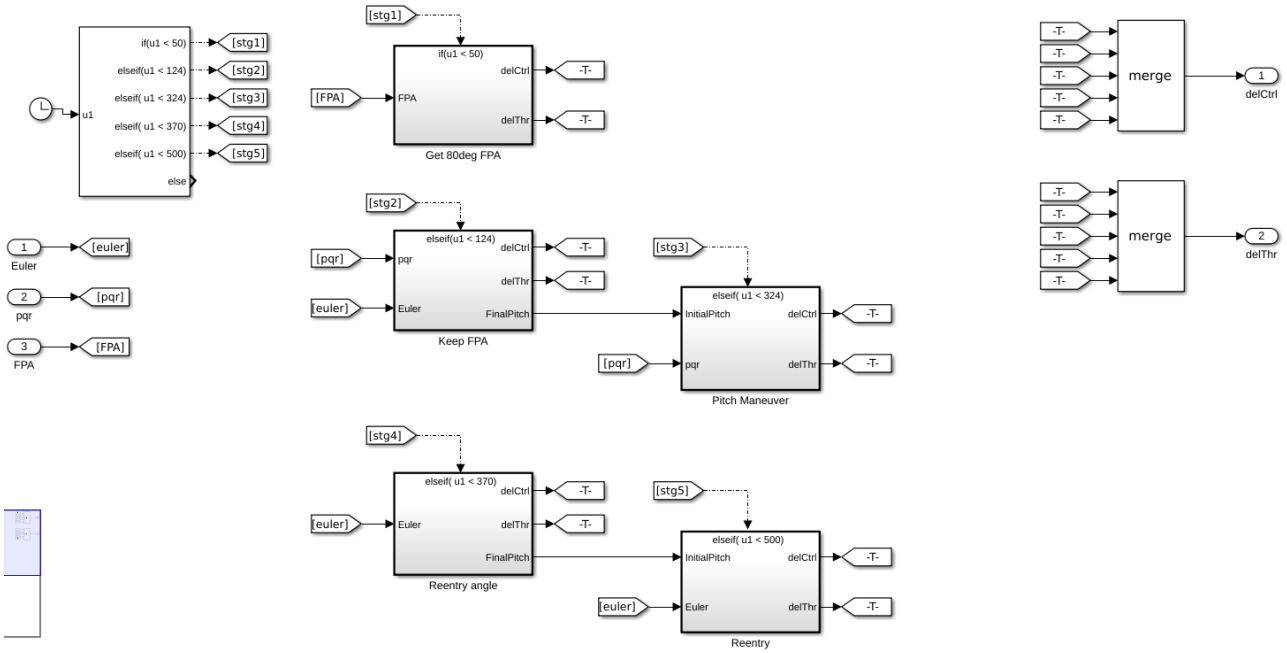

Figure 3.1: Top-level Simulink model of the spacecraft controller.

The pitch control thrusters are modeled as an ideal pure-torque source. Two nozzles are located symmetrically at ±3 ft from the center of gravity along the body-x axis. Each nozzle produces an equal and opposite vertical force, generating a net pitching moment about the body-y axis while canceling translational effects. The flight control system consists of 3 key stages, each responsible for a specific flight regime.

3.1 Stage 1 - Climb

3.1.1 Part 1 - Achieving an 80° Flight Path Angle

Following a stabilized drop of 2 seconds, the rocket engine ignites and the vehicle initiates a climb. A PID controller regulates the elevator deflection based on a 1D lookup table for the Flight Path Angle (FPA), with the goal of reaching 80° while staying within a load factor envelope of $-3g$ to $5g$. This phase occurs within the first 40 seconds of flight.

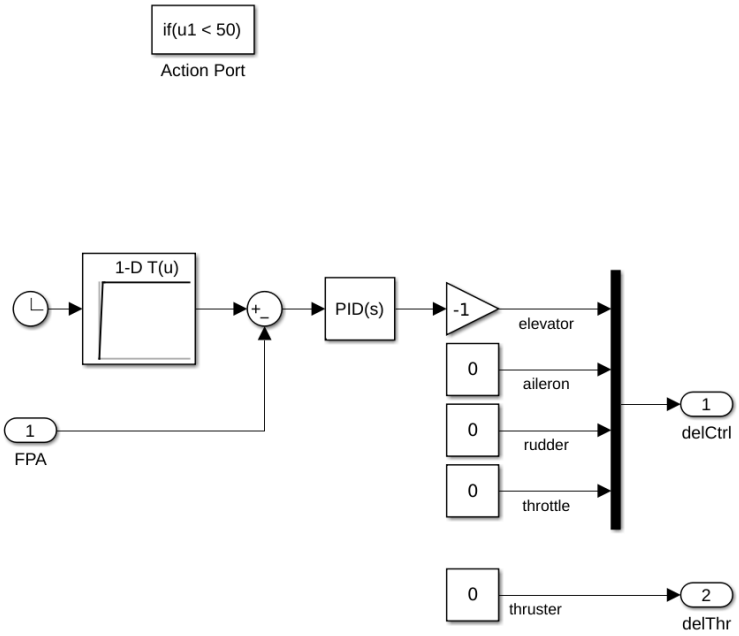

Figure 3.2: Simulink model: Stage 1 (Below 5,000 ft altitude).

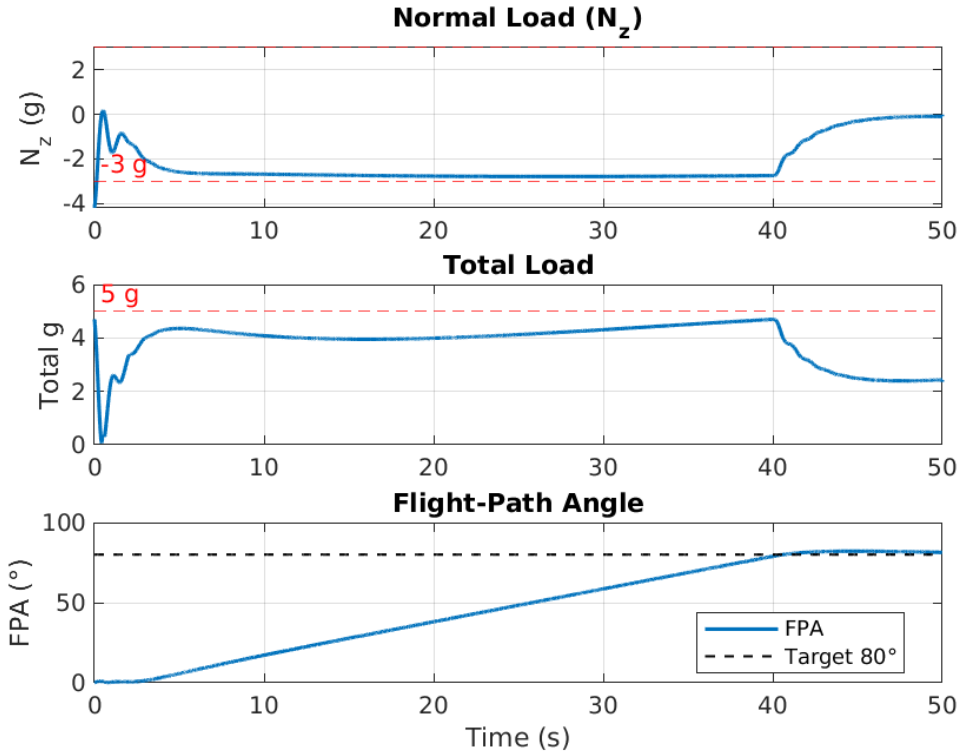

Figure 3.3: Climb phase results: Reaching 80° FPA.

3.1.2 Part 2 – Maintaining the Flight Path Angle

Once the FPA reaches 80°, it is held constant until the vehicle reaches 400,000 ft. This is achieved by keeping the difference between pitch angle θ and angle of attack α constant, maintaining a zero pitch rate q:

$$\gamma = \theta - \alpha \tag{3.1}$$

A PID controller minimizes the pitch rate to hold this configuration. This strategy is effective within a $\pm 4°$ tolerance, as shown in Figure 3.5.

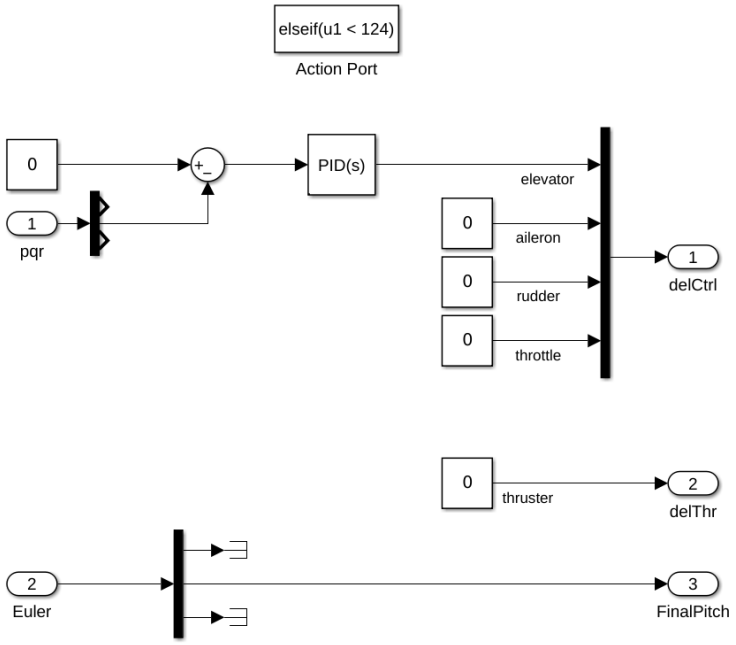

Figure 3.4: Simulink model: Stage 2 (Below 124,000 ft altitude).

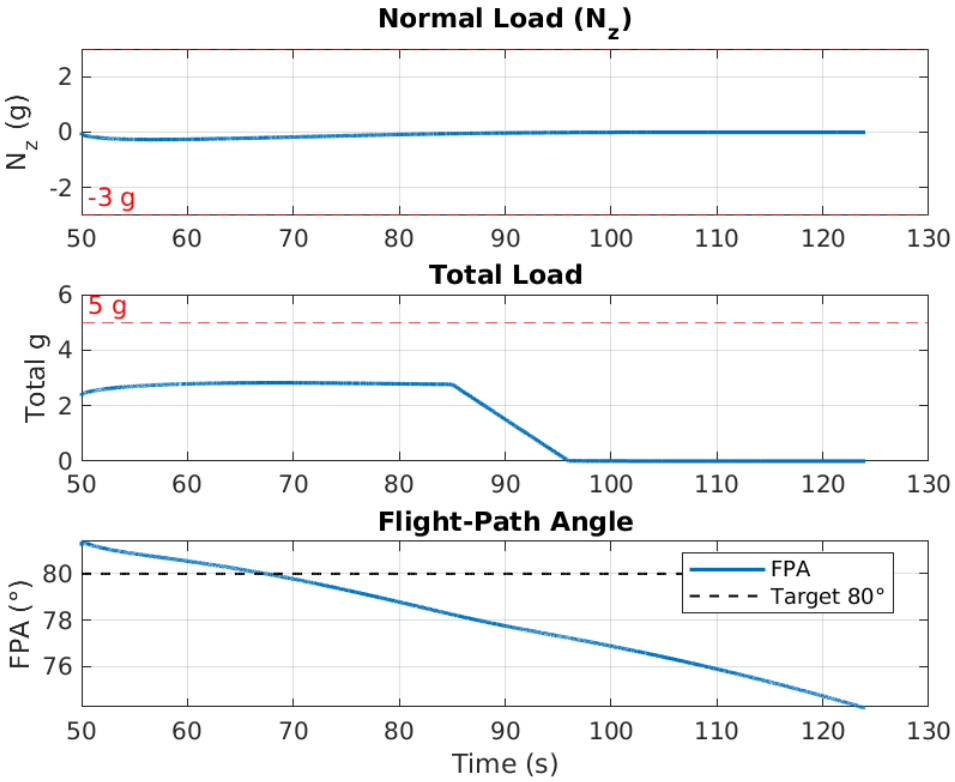

Figure 3.5: Climb phase results: Maintaining FPA.

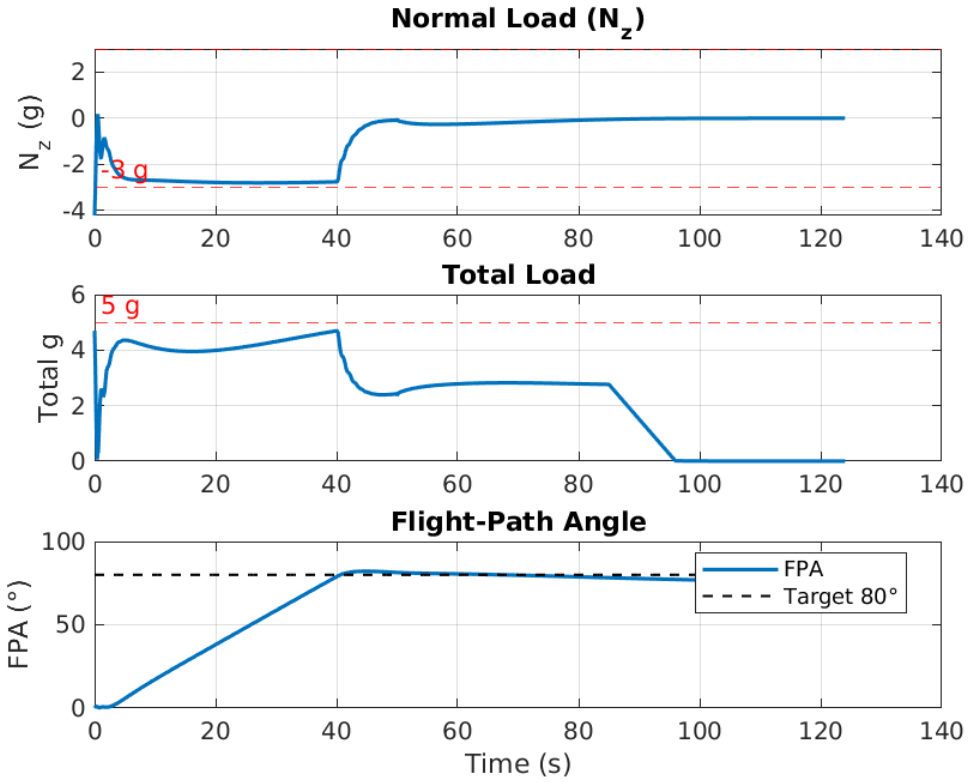

Figure 3.6: Complete climb profile with FPA regulation and g-load envelope.

3.2 Stage 2 - Pitch Maneuver

At altitudes above 400,000 ft, a 360° positive and negative pitch maneuver is executed for passenger visibility. A reference pitch value is defined via a lookup table, and the corresponding pitch rate is derived. A PD controller regulates the torque-generating thrusters to follow this trajectory.

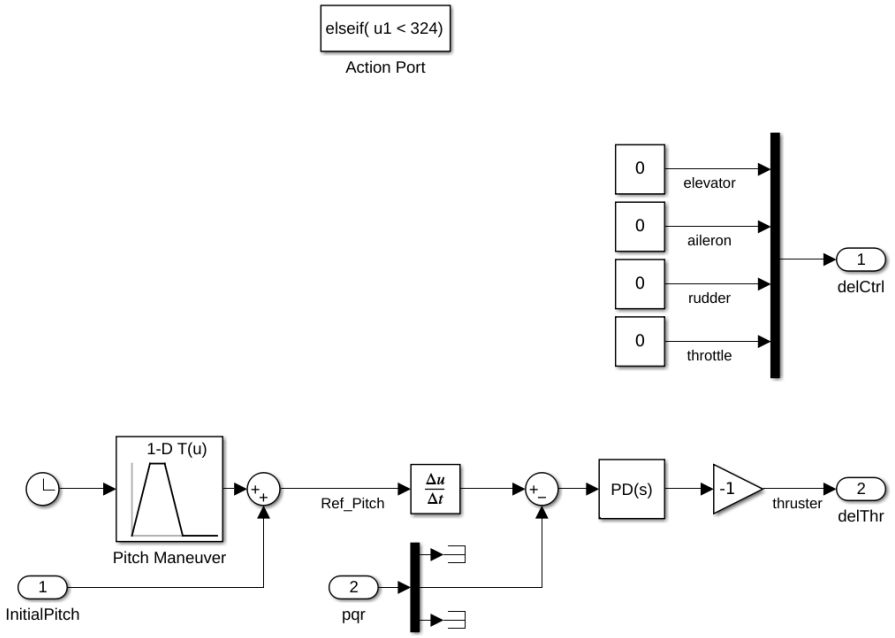

Figure 3.7: Simulink model: Stage 3 (Pitch maneuver control).

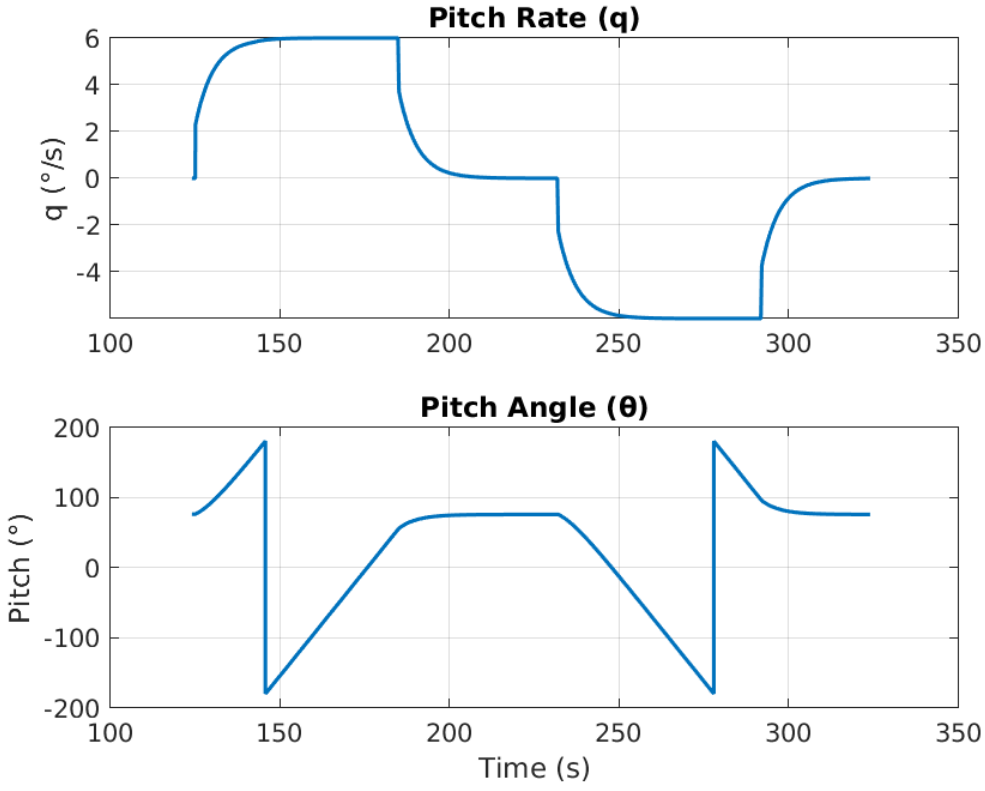

Figure 3.8: Pitch maneuver execution between 130–330 seconds.

3.3 Stage 3 – Reentry Phase

3.3.1 Part 1 – Controlled Reentry Pitch Angle

To minimize heating and g-loading, a controlled pitch descent is initiated with a target pitch angle of $-50°$. A PID controller is used to maintain this orientation during atmospheric reentry.

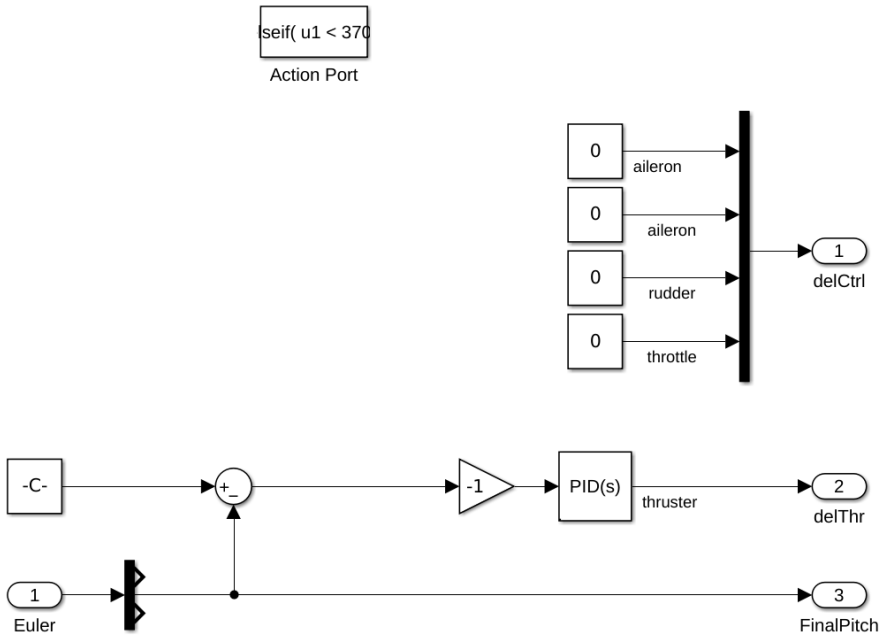

Figure 3.9: Simulink model: Stage 4 (Controlled reentry pitch).

3.3.2 Part 2 - Reentry

To further reduce g-loading, the pitch angle is gradually increased in phases ($-50°$, $-55°$, $-80°$, $-90°$) via a time-based lookup table. Thrusters are turned off at 450 seconds, transitioning the vehicle into a passive glide descent.

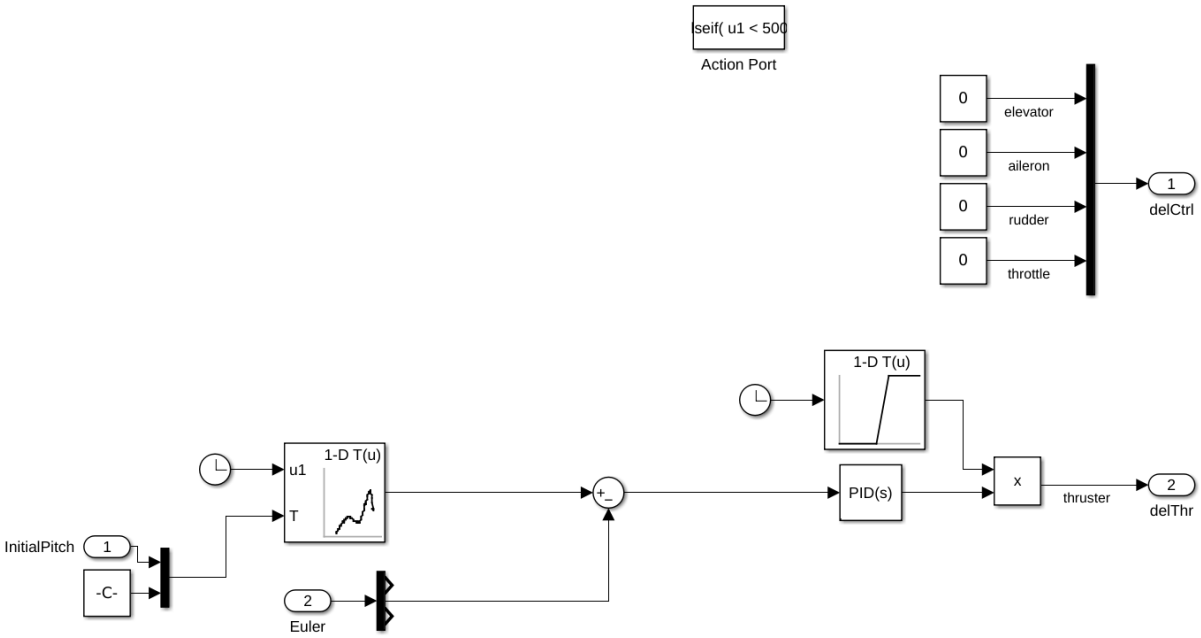

Figure 3.10: Simulink model: Stage 5 (Final reentry phase).

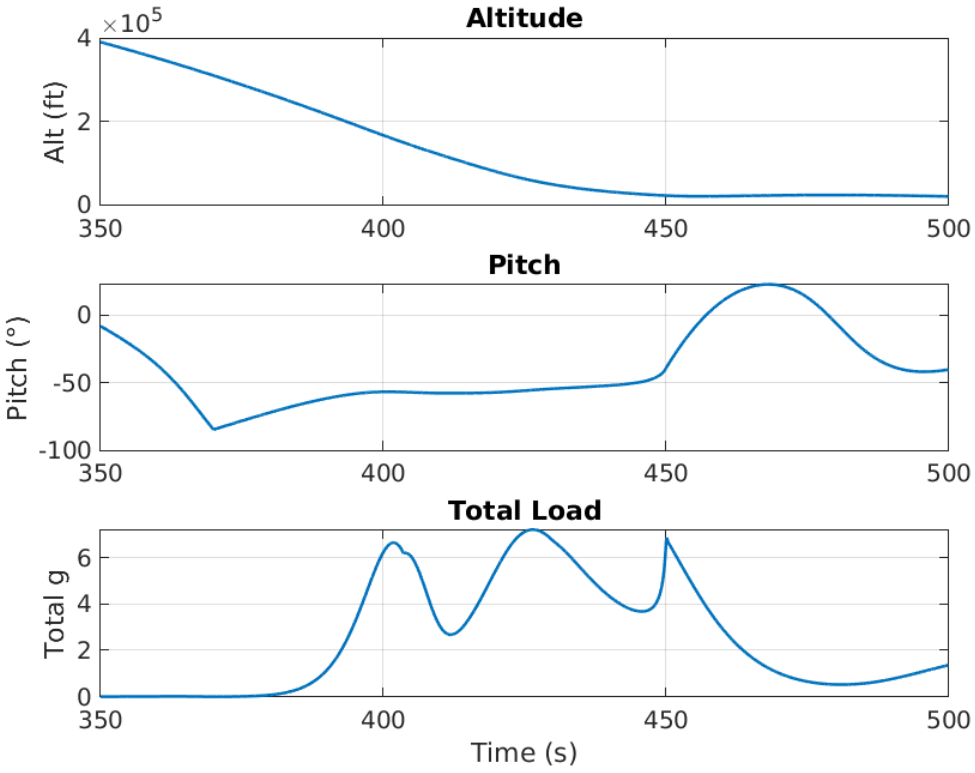

Figure 3.11: Reentry profile with pitch modulation to minimize g-load and thermal stress.

3.4 Flight Overview

The complete simulation spans 500 seconds, where the spacecraft reaches an apogee of 600,000 ft and successfully returns to Earth.

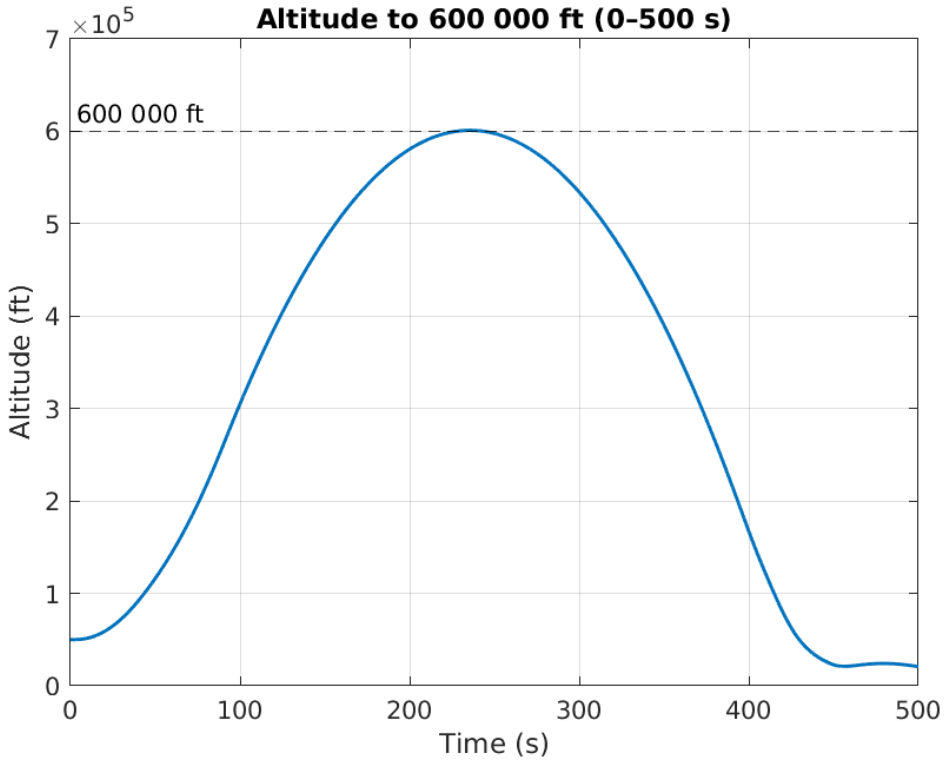

Figure 3.12: Altitude profile showing ascent to 600,000 ft and descent.

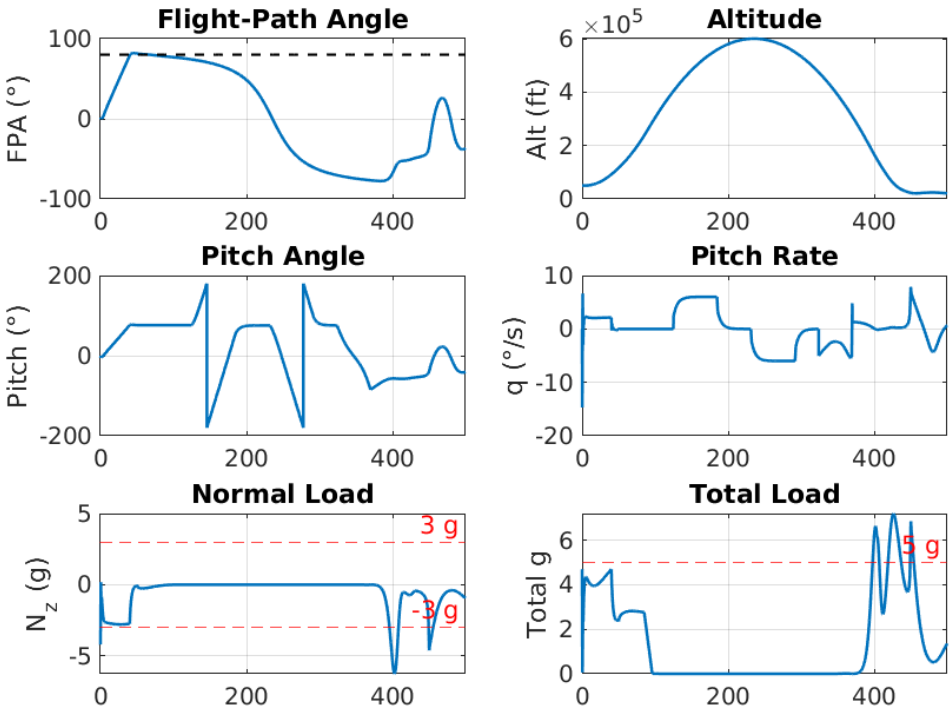

Figure 3.13: Full flight simulation results.

Chapter 4

Lateral-Directional Control Tasks

Chapter Objectives

1. **Establish Positive Aerodynamic Control and Execute a 180° Heading Change:** Demonstrate stable flight dynamics and control effectiveness. Perform a controlled turn to reverse direction.

2. **Navigate to the Heading Alignment Cone Waypoint:** Compute and follow a trajectory to a designated waypoint, passing within 500 feet at any altitude.

This chapter presents the continuation of the spacecraft flight simulation, following the reentry phase. The flight modeled here begins with the vehicle in a stable aerodynamic configuration. Although the platform is a modified, rocket-powered Navion model, this phase is performed entirely in a glide configuration. The top-level Simulink controller used in this segment is shown in Figure 4.1.

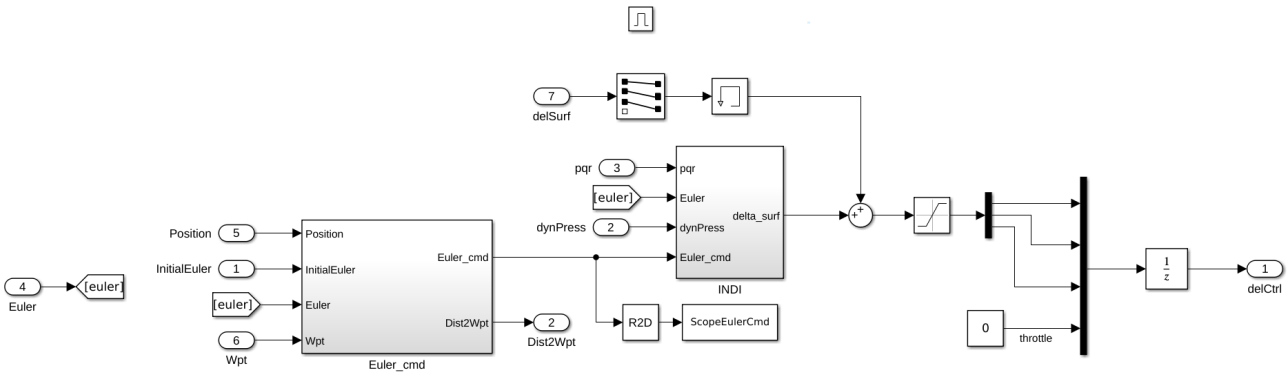

Figure 4.1: Top-level lateral-directional control architecture in Simulink.

The lateral-directional control system consists of two primary components: `Euler_cmd`, which computes the desired bank and pitch angles for the two stages, and `INDI`, which implements an Incremental Nonlinear Dynamic Inversion (INDI) controller to track those commands. The structure of `Euler_cmd` is shown in Figure 4.2.

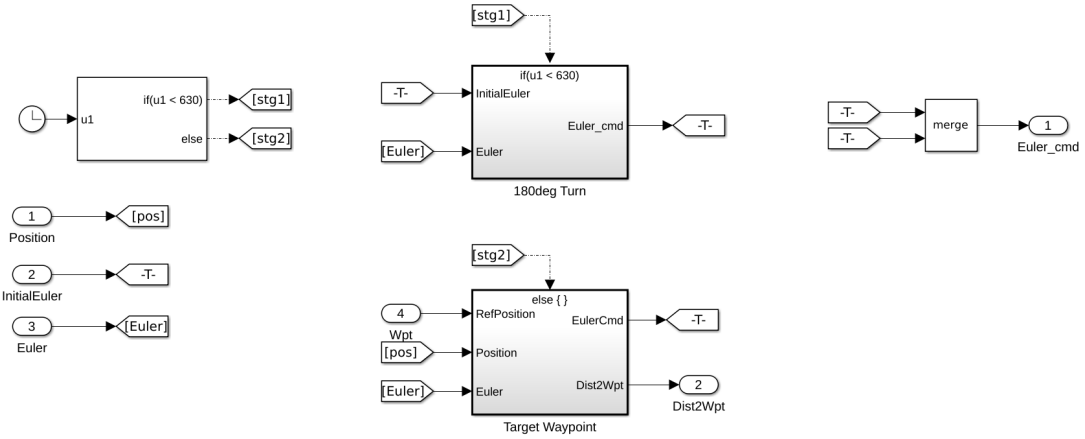

Figure 4.2: Euler angle command generation block.

4.1 Incremental Nonlinear Dynamic Inversion (INDI)

The INDI controller tracks commanded Euler angles using a formulation based on nonlinear dynamic inversion. Consider the general nonlinear first-order MIMO dynamic model:

$$\dot{\mathbf{x}} = \mathbf{f}(\mathbf{x}, \mathbf{p}) + \mathbf{G}(\mathbf{x}, \mathbf{p})\mathbf{u} \tag{4.1}$$

Solving for the control input $\mathbf{u}$ by introducing a virtual outer-loop input $\boldsymbol{\nu}$:

$$\mathbf{u} = \mathbf{G}^{-1}(\hat{\mathbf{x}}, \hat{\mathbf{p}}) \left[\boldsymbol{\nu} - \mathbf{f}(\hat{\mathbf{x}}, \hat{\mathbf{p}})\right] \tag{4.2}$$

According to Lombaerts et al. [2], this results in a system that behaves like a pure integrator by canceling the nonlinear aircraft dynamics. The incremental form computes changes in control inputs relative to previous system conditions, using a linear controller (e.g., PID) to define $\boldsymbol{\nu}$ based on tracking errors in Euler angles.

The aerodynamic moments are defined as:

$$\mathbf{M}_{\text{aero}} = \begin{bmatrix} L_{\text{aero}} \\ M_{\text{aero}} \\ N_{\text{aero}} \end{bmatrix} = \begin{bmatrix} bC_l \\ \bar{c}C_m \\ bC_n \end{bmatrix} \bar{q}S \tag{4.3}$$

The required moment increments from the desired angular accelerations are:

$$\begin{bmatrix} dL_{\text{req}} \\ dM_{\text{req}} \\ dN_{\text{req}} \end{bmatrix} = \begin{bmatrix} I_{XX}(\dot{p}_{\text{req}} - \hat{p}_0) - I_{XZ}(\dot{r}_{\text{req}} - \hat{r}_0) \\ I_{YY}(\dot{q}_{\text{req}} - \hat{q}_0) \\ I_{ZZ}(\dot{r}_{\text{req}} - \hat{r}_0) - I_{XZ}(\dot{p}_{\text{req}} - \hat{p}_0) \end{bmatrix} \tag{4.4}$$

And the relationship between aerodynamic moment increments and control deflections is:

$$\begin{bmatrix} dL_{\text{req}} \\ dM_{\text{req}} \\ dN_{\text{req}} \end{bmatrix} = \begin{bmatrix} bC_{l_{\delta_a}} & 0 & bC_{l_{\delta_r}} \\ 0 & \bar{c}C_{m_{\delta_e}} & 0 \\ bC_{n_{\delta_a}} & 0 & bC_{n_{\delta_r}} \end{bmatrix} \bar{q}S \cdot \begin{bmatrix} \Delta\delta_a \\ \Delta\delta_e \\ \Delta\delta_r \end{bmatrix} \tag{4.5}$$

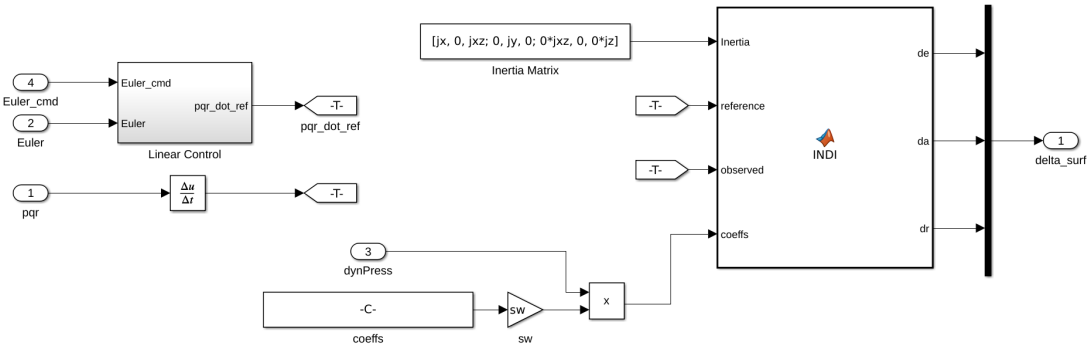

Figure 4.3: INDI implementation in Simulink for lateral-directional control.

4.2 Stage 4 – Heading Reversal 180°

To reverse the heading, a bias of 180° is added to the current heading angle. A heading error is then computed and passed through a 1-D lookup table to define the desired bank angle. The lookup table uses breakpoints at [0, 10, 180] degrees and outputs [0, 5, 25] degrees of bank angle. Simultaneously, a time-based lookup table drives the pitch angle from its current value to 1°, in order to reduce the rate of descend.

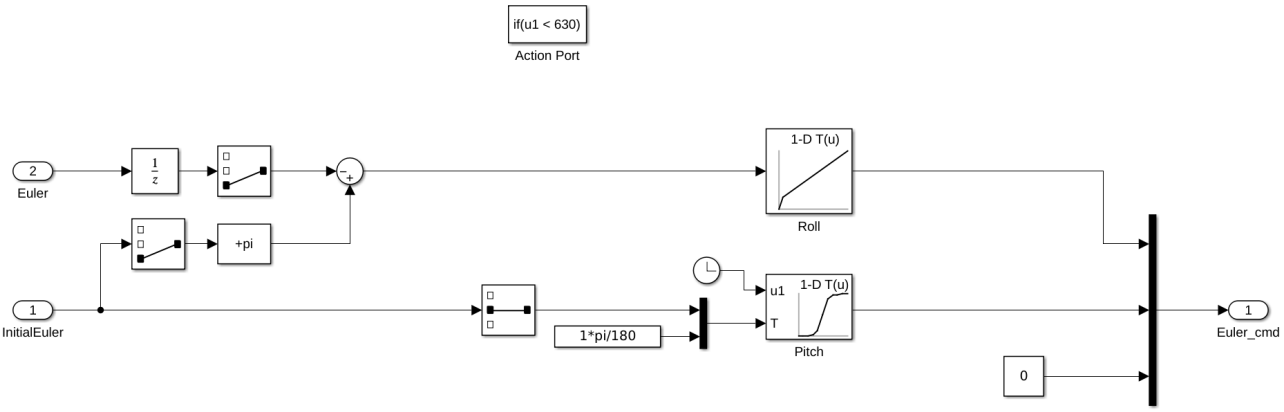

Figure 4.4: Euler command logic for heading reversal maneuver.

The controller successfully tracks the commanded bank and pitch angles, achieving the full 180° turn as shown in Figure 4.5.

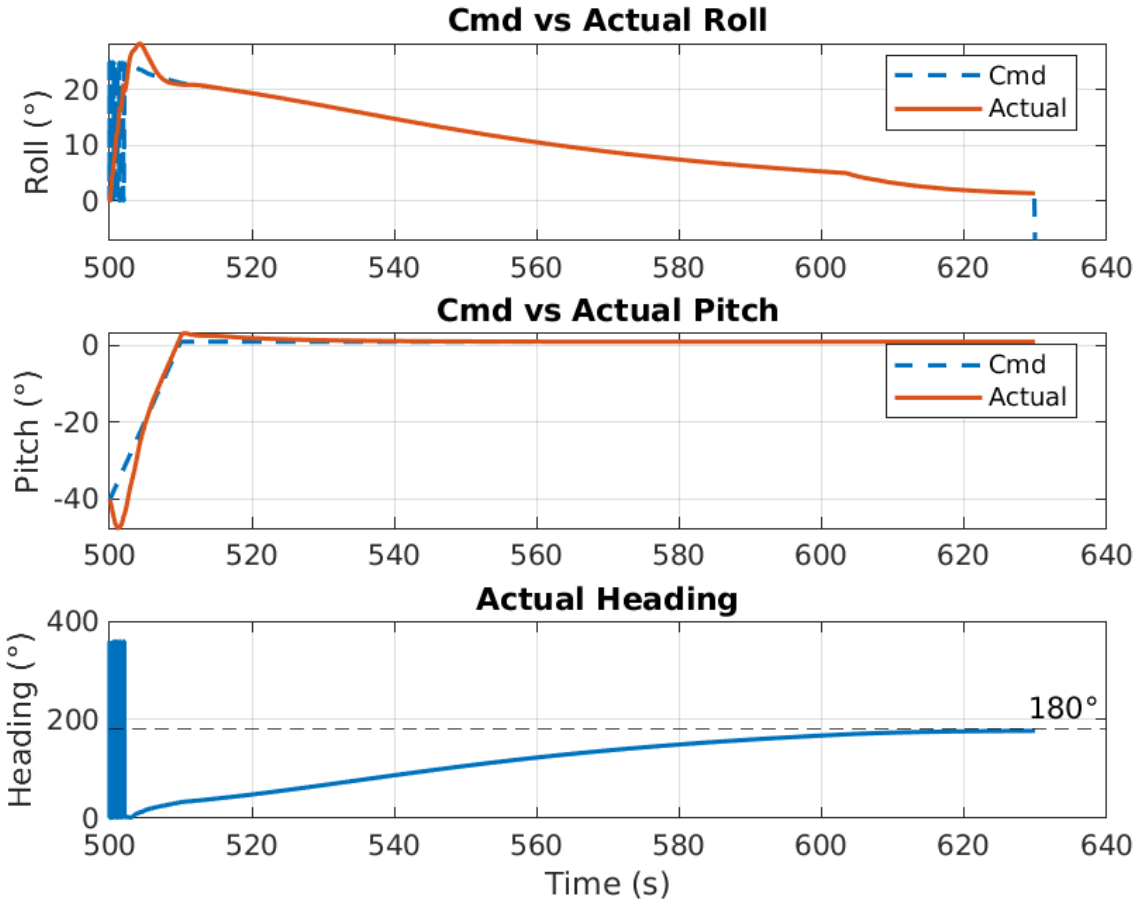

Figure 4.5: Euler angle tracking during 180° heading reversal.

4.3 Stage 5 - Waypoint Tracking

After the heading reversal, the vehicle is directed toward a target waypoint located at (N = 561,000 ft, $E = -5{,}000$ ft). The pitch angle command remains at 1°, while the bank angle command is computed using a heading error derived from the difference between the current and desired headings. The desired heading is calculated via:

$$\psi_{\text{des}} = \text{atan2}(\text{Error}_E, \text{Error}_N)$$

This heading error feeds into a lookup table to compute the desired bank angle. The complete implementation is shown in Figure 4.6.

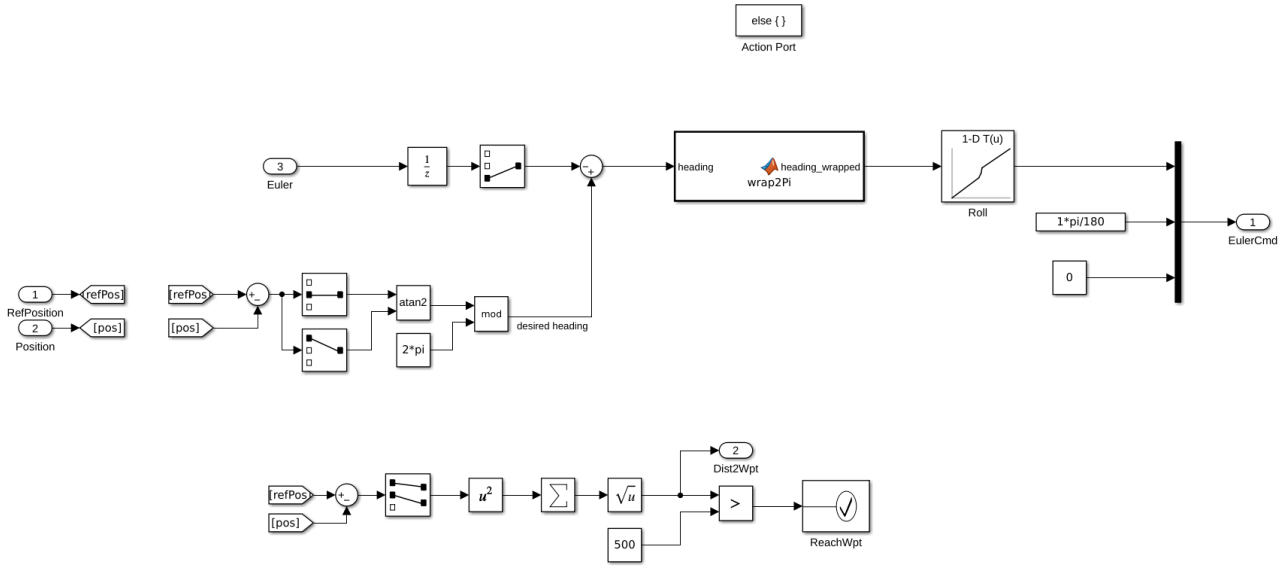

Figure 4.6: Euler command logic for waypoint navigation.

To terminate the simulation, a proximity check asserts when the aircraft is within 500 ft of the waypoint. Euler tracking performance is shown in Figure 4.7

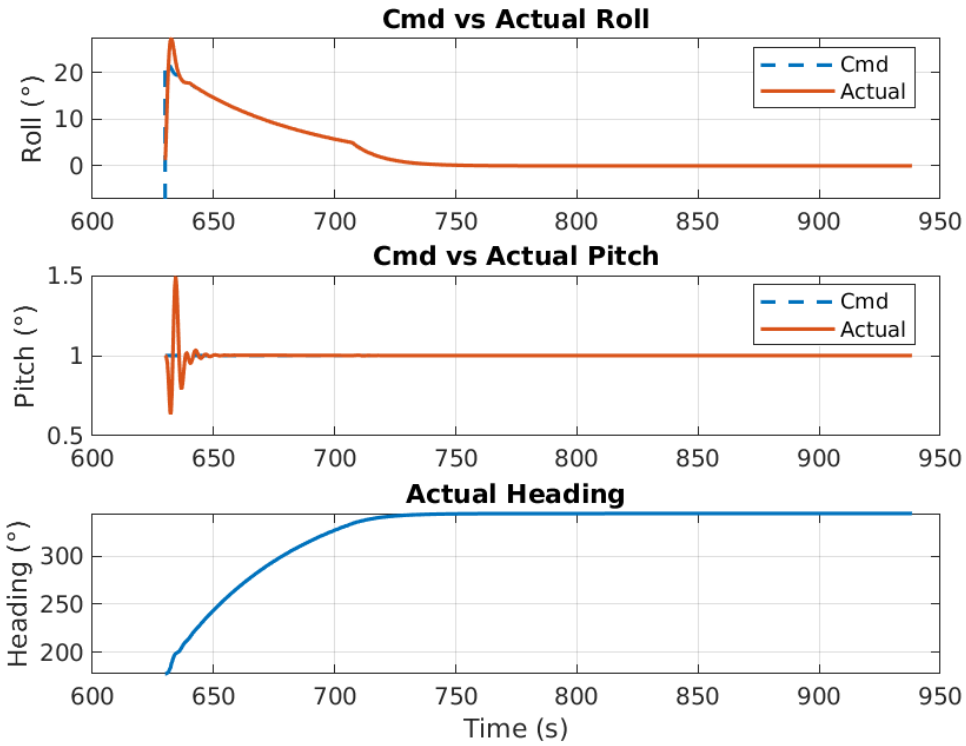

Figure 4.7: Euler angle tracking while navigating to the waypoint.

4.4 Flight Overview

Figure 4.8 shows the complete Euler angle tracking across both lateral-directional phases of flight: the heading reversal and waypoint alignment, and the flight path trajectory is presented in Figure 4.9..

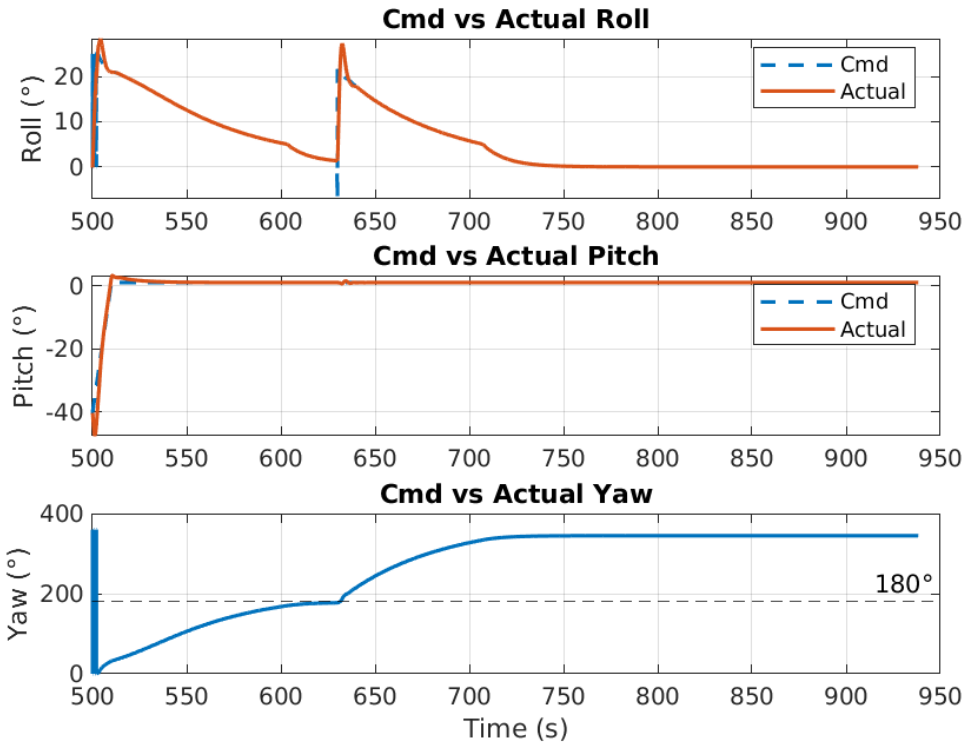

Figure 4.8: Complete flight profile: commanded vs. actual Euler angles.

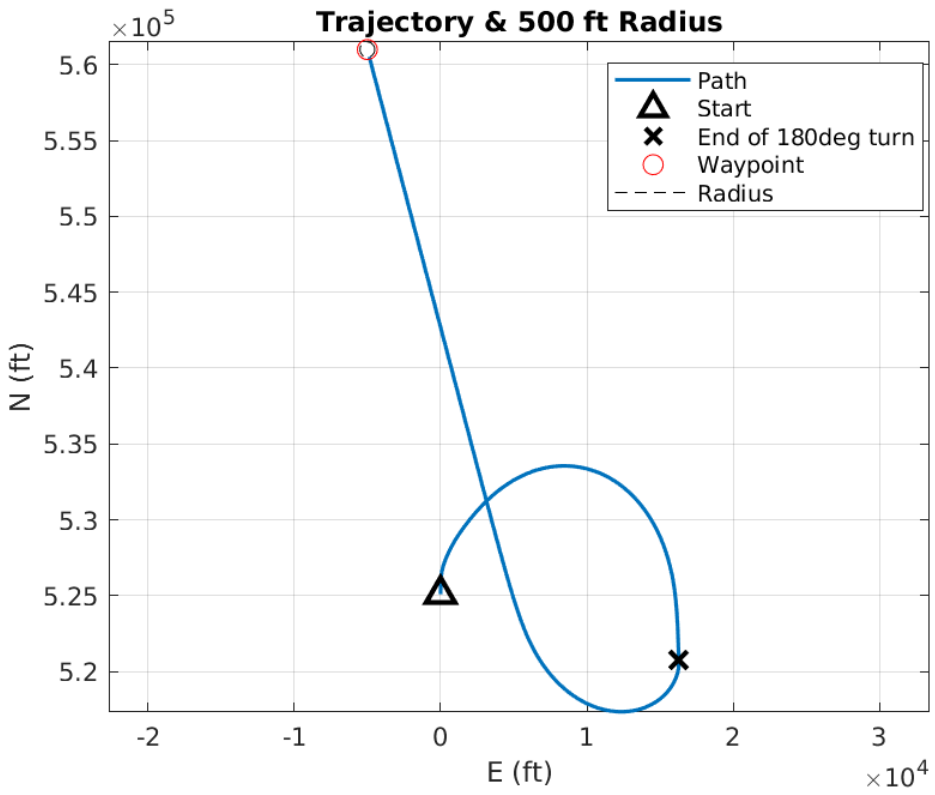

Figure 4.9: Trajectory plot showing successful approach to the waypoint.

Part IV

Modeling and Validation

Chapter 5

Introduction

The Cessna 182Q is a single-engine, fixed-wing aircraft manufactured by Cessna. It features a high-wing configuration and a four-seat cabin. The aircraft is powered by a Teledyne Continental O-470-U engine, which produces 230 brake horsepower at 2400 RPM, and it is equipped with a McCauley C2A34C204/90DCB-8 constant speed propeller [3]. An image of the aircraft is shown in Figure 5.1.



Figure 5.1: Cessna 182Q Aircraft

This chapter establishes the foundation for the development of a mathematical model of the Cessna 182Q. Multiple aircraft parameters, including geometric characteristics, control surface deflections, and aerodynamic reference locations, are determined. The locations of key instruments, such as air data sensors and the Inertial Measurement Unit (IMU), are measured relative to the datum defined by Cessna. Additionally, the aircraft's weight and center of gravity are computed. Finally, the thrust vector is expressed in terms of the body-fixed coordinate system.

5.1 Aircraft Geometry

The geometry of the Cessna 182Q as well as it's control surface deflection information are shown in Table 5.1 and Table 5.2.

Table 5.1: Cessna 182Q Aircraft Geometry

Overall Dimensions	
Dimension	**Imperial**
Wingspan	36 ft
Length	28 ft
Height	9 ft 3 in
Wing Dimensions	
Wing Area	174 ft^2
Mean Aerodynamic Chord	4.9 ft
Aspect Ratio	7.44
Landing Gear	
Track	9 ft
Wheelbase	5.54 ft
Propeller Ground Clearance	0.91 ft

Table 5.2: Control Surface Deflections for Cessna 182Q

Control Surface	**Deflection Direction**	**Deflection (deg)**
Aileron	Trailing edge up	$20° \pm 2°$
	Trailing edge down	$15° \pm 2°$
Elevator	Trailing edge up	$26° \pm 1°$
	Trailing edge down	$17° \pm 1°$
Elevator Trim Tab	Nose up at elevator neutral	$25° \pm 2°$
	Nose down at elevator neutral	$15° \pm 1°$
Rudder	Left	$24° \pm 1°$
	Right	$24° \pm 1°$
Rudder (perpendicular to hinge line)	Left	$27°13' \pm 1°$
	Right	$27°13' \pm 1°$
Flaps	Flap setting	Down $40° + 1°, -2°$

5.2 Powerplant and Propeller

The Cessna 182Q is equipped with the following engine and propeller:

- **Engine Manufacturer and Designation:** Teledyne Continental O-470-U (230 bhp @ 2400 RPM)
- **Propeller Manufacturer and Designation:** McCauley Accessory Division C2A34C204/90DCB-8

5.3 Reference Datum

The reference datum is defined as an imaginary vertical plane from which all horizontal distances are measured for balance purposes. For the Cessna 182Q is defined as per page 2-7, Section 2 of POH (Pilot Operating Handbook), the **reference datum is the Front face of the firewall** [3].

For reference, distances measured with respect to the datum are defined in a right-handed coordinate system as follows:

- **X-axis**: Distances are measured along the longitudinal axis of the aircraft.
  - Negative X values correspond to locations forward of the datum (toward the nose).
  - Positive X values correspond to locations aft of the datum (toward the tail).
- **Y-axis**: Distances are measured laterally from the aircraft centerline.
  - Positive Y values correspond to locations to the right of the pilot.
  - Negative Y values correspond to locations to the left of the pilot.
- **Z-axis**: Distances are measured vertically from the datum.
  - Positive Z values correspond to locations above the datum.
  - Negative Z values correspond to locations below the datum.

5.4 Instrumentation Locations

The positions of key sensors on the aircraft are measured with respect to the datum defined by Cessna and are as follows:

Table 5.3: Positions of Air Data Instruments and IMU

Instrument	X (in)	Y (in)	Z (in)
Angle of Attack Indicator	-16.3	-203.9	-51.65
Angle of Sideslip Indicator	-6.05	-206.03	-49.4
Pitot-Static	-32.05	-206.03	-50.65
IMU	90.9	-0.3	-2.7

5.5 Weight and Balance

This section describes the procedure for establishing the basic empty weight and moment of the airplane. Sample forms are provided for reference. Procedures for calculating the weight and moment for various operations are also provided. A comprehensive list of all Cessna equipment available for this airplane is included at the back of this section.

It should be noted that specific information regarding the weight, arm, moment, and installed equipment list for this airplane can only be found in the appropriate weight and balance records carried in the airplane.

It is the responsibility of the pilot to ensure that the airplane is loaded properly.

AIRPLANE WEIGHING PROCEDURES

1. Preparation
   (a) Inflate tires to recommended operating pressures.
   (b) Remove the fuel tank sump quick-drain fittings and fuel selector valve drain plug to drain all fuel.
   (c) Remove oil sump drain plug to drain all oil.
   (d) Move sliding seats to the most forward position.
   (e) Raise flaps to the fully retracted position.
   (f) Place all control surfaces in neutral position.
2. Leveling
   (a) Place scales under each wheel (minimum scale capacity, 1000 pounds).
   (b) Deflate nose tire and/or lower or raise the nose strut to properly center bubble on level (see Table 5.4).
3. Weighing
   (a) With the airplane level and brakes released, record the weight shown on each scale. Deduct the tare, if any, from each reading.
4. Measuring
   (a) Obtain measurement A by measuring horizontally (along the airplane center line) from a line stretched between the main wheel centers to a plumb bob dropped from the firewall.
   (b) Obtain measurement B by measuring horizontally and parallel to the airplane center line, from the center of the nose wheel axle, left side, to a plumb bob dropped from the line between the main wheel centers. Repeat on the right side and average the measurements.
5. Using weights from item 3 and measurements from item 4, the airplane weight and C.G. can be determined.
6. Basic Empty Weight may be determined by completing Table 5.4.

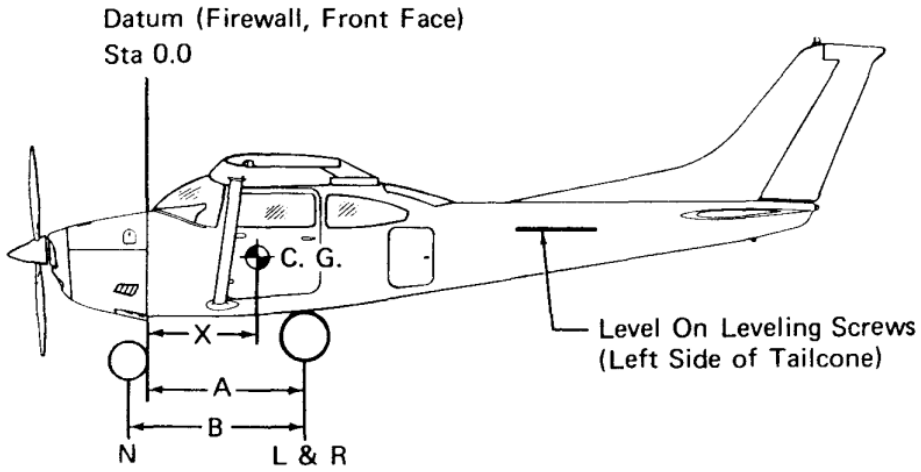

Scale Position	**Scale Reading**	**Tare**	**Symbol**	**Net Weight**
Left Wheel			L	
Right Wheel			R	
Nose Wheel			N	
Sum of Net Weights (As Weighed)			W	

$$\text{X} = \text{ARM} = (\text{A}) - \frac{(\text{N}) \times (\text{B})}{(\text{W})}; \qquad \text{X} = (\quad) - \frac{(\quad) \times (\quad)}{(\quad)} = (\quad) \text{ IN.}$$

Table 5.4: Sample Airplane Weighing

Item	**Weight (Lbs.)**	**X C.G. Arm (In.) =**	**Moment/1000 (Lbs.-In.)**
Airplane Weight (From Item 5)			
No Oil Filter (12 Qts at 7.5 Lbs/Gal)		-15.0	
With Oil Filter (13 Qts at 7.5 Lbs/Gal)		-15.0	
Unusable Fuel (4 Gal at 6 Lbs/Gal)	24	48.0	1.2
Equipment Changes			
Airplane Basic Empty Weight			

WEIGHT AND BALANCE

The following information will enable you to operate your Cessna within the prescribed weight and center of gravity limitations. To figure weight and balance, use the Sample Problem, Loading Graph, and Center of Gravity Moment Envelope as follows:

Take the basic empty weight and moment from appropriate weight and balance records carried in your airplane, and enter them in the column titled YOUR AIRPLANE on the Sample Loading Problem.

NOTE

In addition to the basic empty weight and moment noted on these records, the C.G. arm (fuselage station) is also shown, but need not be used on the Sample Loading Problem. The moment which is shown must be divided by 1000 and this value used as the moment/1000 on the loading problem.

Use the Loading Graph to determine the moment/1000 for each additional item to be carried; then list these on the loading problem.

NOTE

Loading Graph information for the pilot, passengers, baggage/ cargo and hatshelf is based on seats positioned for average occupants and baggage/ cargo or hatshelf items loaded in the center of these areas as shown on the Loading Arrangements diagram. For loadings which may differ from these, the Sample Loading Problem lists fuselage stations for these items to indicate their forward and aft C. G. range limitation (seat travel and baggage / cargo or hatshelf area limitation). Additional moment calculations, based on the actual weight and C.G. arm (fuselage station) of the item being loaded, must be made if the position of the load is different from that shown on the Loading Graph.

Total the weights and moments/1000 and plot these values on the Center of Gravity Moment Envelope to determine whether the point falls within the envelope, and if the loading is acceptable.

BAGGAGE AND CARGO TIE-DOWN

A nylon baggage net having six tie-down straps is provided as standard equipment to secure baggage in the area aft of the rear seat and on the hatshelf. Six eyebolts serve as attaching points for the net. Two eyebolts for the forward tie-down straps are mounted on the cabin floor near each sidewall just forward of the baggage door approximately at station 92; two center eyebolts mount on the floor slightly inboard of each sidewall just aft of the baggage door approximately at station 109; the two aft eyebolts secure at the top of the rear baggage wall at station 124. If a child's seat is installed, only the center and aft eyebolts will be needed for securing the net in the area remaining behind the seat. A placard on the baggage door defines the weight limitations in the baggage areas.

A cargo tie-down kit consisting of nine tie-down attachments is available if it is desired to remove the rear seat (and child's seat. if installed) and utilize the rear cabin area to haul cargo. Two tie-down attachments clamp to the aft end of the two outboard front seat rails

and are locked in place by a bolt which must be tightened to a minimum of fifty inch pounds. Seven tie-down attachments bolt to standard attach points in the cabin floor, including three rear seat mounting points. The seven attach points are located as follows: two are located slightly inboard and just aft of the rear doorposts approximately at station 69; two utilize the aft outboard mounting points of the rear seat; one utilizes the rearmost mounting point of the aft center attach point for the rear seat approximately at station 84 (a second mounting point is located just forward of this point but is not used); and two are located just forward of the center baggage net tie-down eyebolts approximately at station 108. The maximum allowable floor loading of the rear cabin area is 200 pounds/ square foot; however, when items with small or sharp support areas are carried, the installation of a 1/4" plywood floor is recommended to protect the airplane structure. The maximum rated load weight capacity for each of the seven tie-downs is 140 pounds and for the two seat rail tie-downs is 100 pounds. Rope, strap, or cable used for tie-down should be rated at a minimum of ten times the load weight capacity of the tie-down fittings used. Weight and balance calculations for cargo in the area of the rear seat, baggage and hatshelf area can be figured on the Loading Graph using the lines labeled 2nd Row Passengers or Cargo and/ or Baggage or Passengers on Child's Seat.

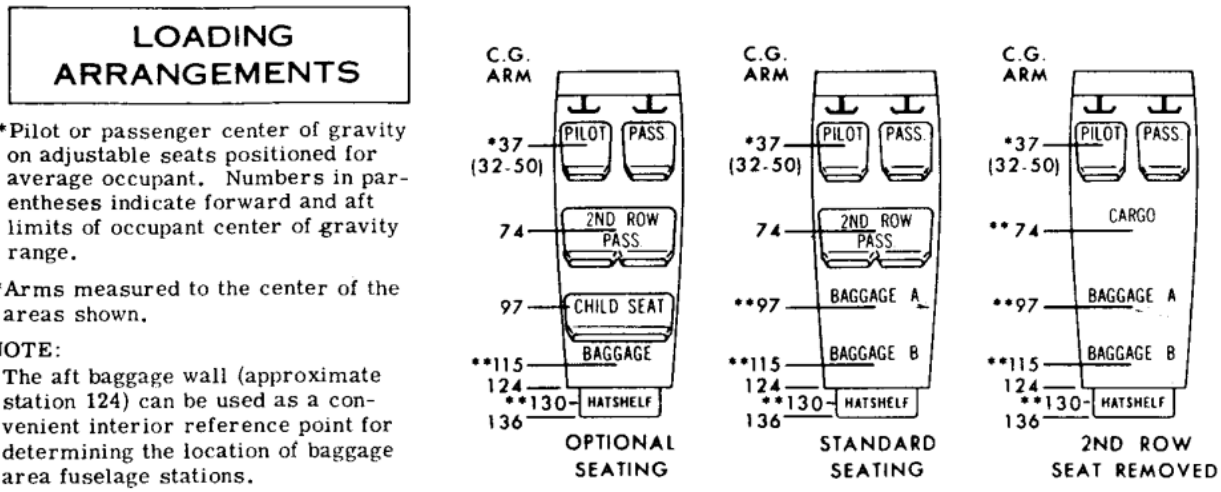

Figure 5.2: Loading Arrangements

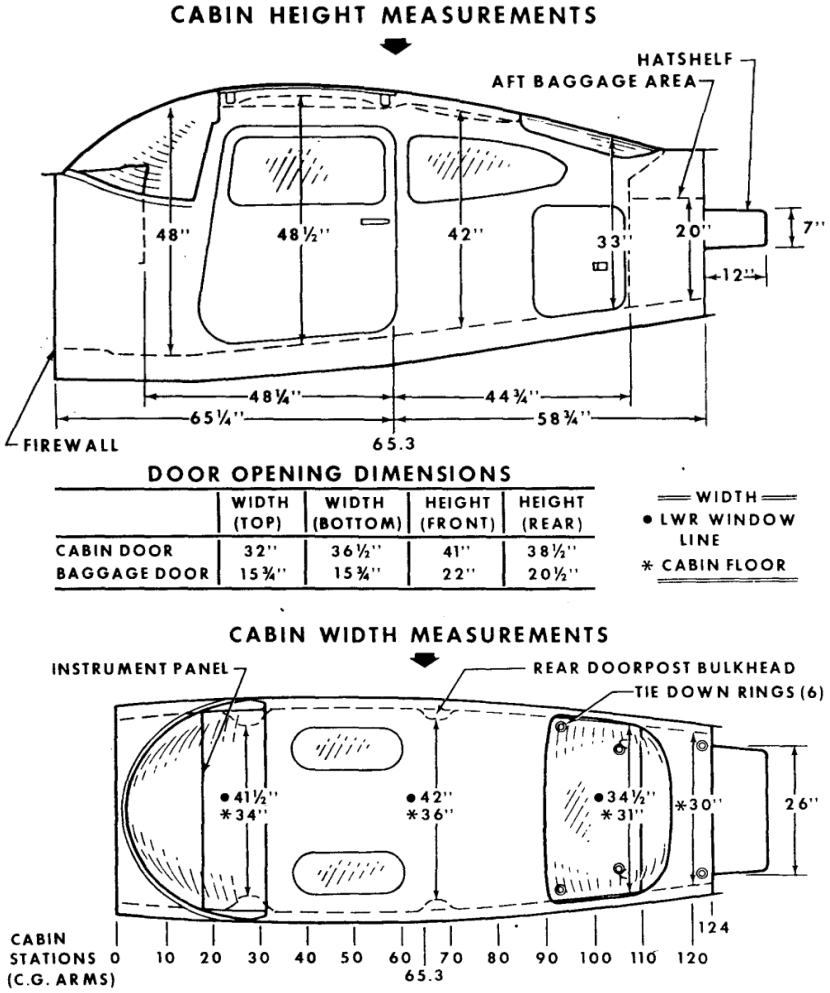

Figure 5.3: Cabin height and width measurements

5.5.1 Weight and Balance Log Entries

The following table provides a historical log of weight and balance changes due to modifications, additions, or removals of aircraft components.

Table 5.5: Weight and Balance Entries

Who	Date	Time	Action	Item	Weight	Arm	Moment
Sitinelli,D	Mar 17 2015	5,308.90	Install	Aircraft re-weighed (with full oil)	1,961.00	37.8631	74,294.58
Johnson,S.	Nov 04 2015	5,308.90	Install	AOA Brackets	0.95	40.0000	38.00
Johnson,S.	Nov 04 2015	5,308.90	Install	AOA Brackets	0.75	54.0000	40.50
Johnson,S.	Nov 04 2015	5,308.90	Install	AOA Brackets	0.87	66.5000	57.86
Sitinelli,D	Dec 16 2015	5,308.90	Remove	GNS 530 Unit	7.00	12.90000	-90.30

The following table summarizes the weight and balance parameters of the Cessna 182Q:

Table 5.6: Basic Aircraft Weight and Balance

Max Weight (lbs)	**Empty Weight (lbs)**	**Useful Load (lbs)**	**CG Location (in)**
2,950.00	1,956.57	993.43	37.9724

The total weight and moment of the aircraft were computed as follows:

$$\text{Total Weight} = 1,956.57 \text{ lbs} \tag{5.1}$$
$$\text{Total Moment} = 74,295.59 \text{ lb-in} \tag{5.2}$$

5.6 Aerodynamic Center Location and Mean Aerodynamic Chord

The Aerodynamic Center (AC) location was determined using the following calculations:

$$c_t = 3.7570 \quad \text{(Tip chord in ft)} \tag{5.3}$$
$$c_r = 5.3346 \quad \text{(Root chord in ft)} \tag{5.4}$$
$$c_b = c_r \quad \text{(Chord at break point)} \tag{5.5}$$

The taper ratios for the inboard and outboard wing sections are given by:

$$\lambda_i = \frac{c_b}{c_r} = 1.0 \tag{5.6}$$
$$\lambda_o = \frac{c_t}{c_b} = 0.7043 \tag{5.7}$$

The wing parameters used in the calculations are:

$$b/2 = 18 \quad \text{(Half wingspan in ft)} \tag{5.8}$$
$$y_b = 6.42 \quad \text{(Spanwise location of break point in ft)} \tag{5.9}$$

To determine the Mean Aerodynamic Chord (MAC), the following formulas were applied for both the inboard and outboard panels:

$$\frac{y_{\text{MAC},x}}{b_x/2} = \frac{1}{3} \cdot \frac{1+2\lambda}{1+\lambda} \tag{5.10}$$

$$\bar{c}_x = \frac{2}{3} c_{r_x} \cdot \frac{1+\lambda+\lambda^2}{1+\lambda} \tag{5.11}$$

$$S_x = (b_x/2) \cdot c_{r_x} \cdot (1+\lambda) \tag{5.12}$$

where x refers to either the inboard or outboard panel. Finally, the overall mean aerodynamic chord and its spanwise location are determined as:

$$\bar{c} = \frac{\bar{c}_i S_i + \bar{c}_o S_o}{S_i + S_o} = 4.88\,\text{ft} \tag{5.13}$$

$$y_{\text{MAC}} = \frac{y_{\text{MAC},i} S_i + (y_{\text{MAC},o} + y_b) S_o}{S_i + S_o} = 8.45\,\text{ft} \tag{5.14}$$

Using the calculated mean aerodynamic chord ($\bar{c}$), the 25% MAC location is computed as follows:

- **MAC**: 4.9 ft (58.8 inches)
- **25% MAC**: 1.225 ft (14.7 inches)
- **Reference from Datum**: Firewall to Leading Edge of the Wing + 25% MAC

$$\text{Location of 25\% MAC} = 2.04\text{ ft} + 1.225\text{ ft} = 3.265\text{ ft} \quad (39.18\text{ inches})$$

The following figures illustrate the computed location of 25% MAC with respect to the datum.

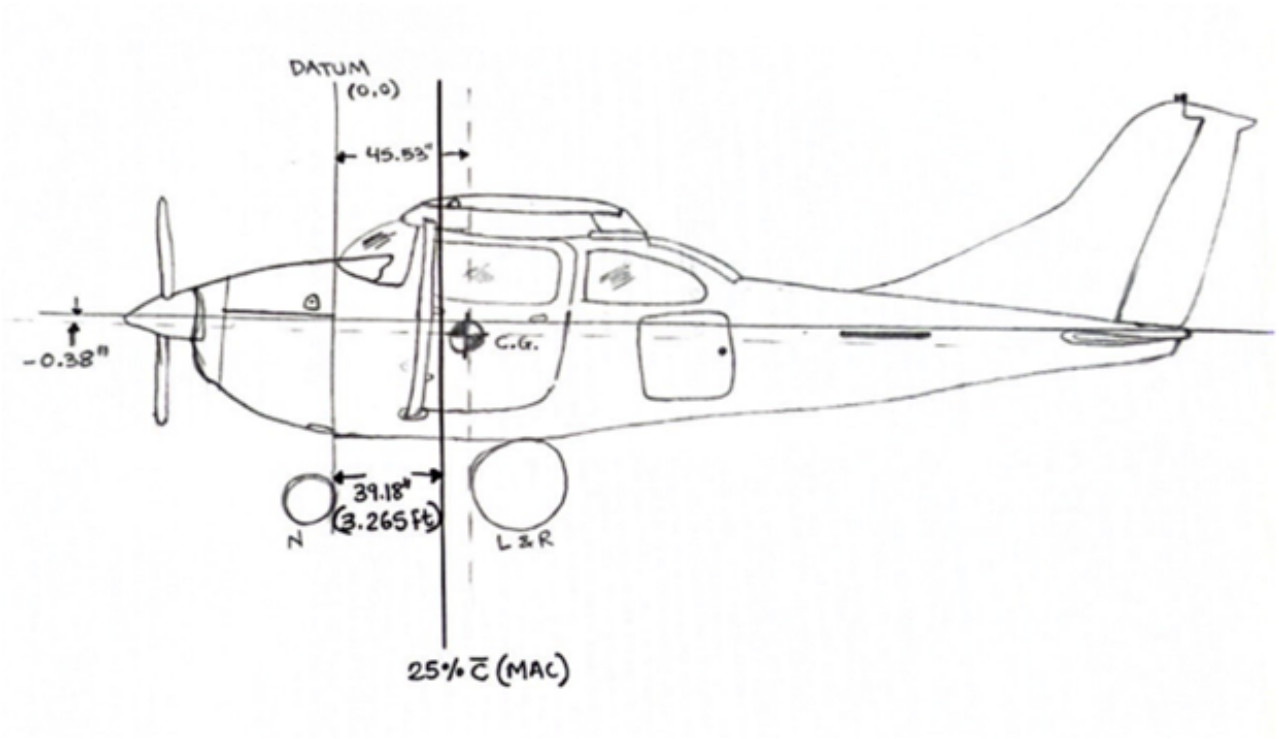

Figure 5.4: The location of 25% $\bar{c}$ with respect to the datum (39.18 inches) - Side view

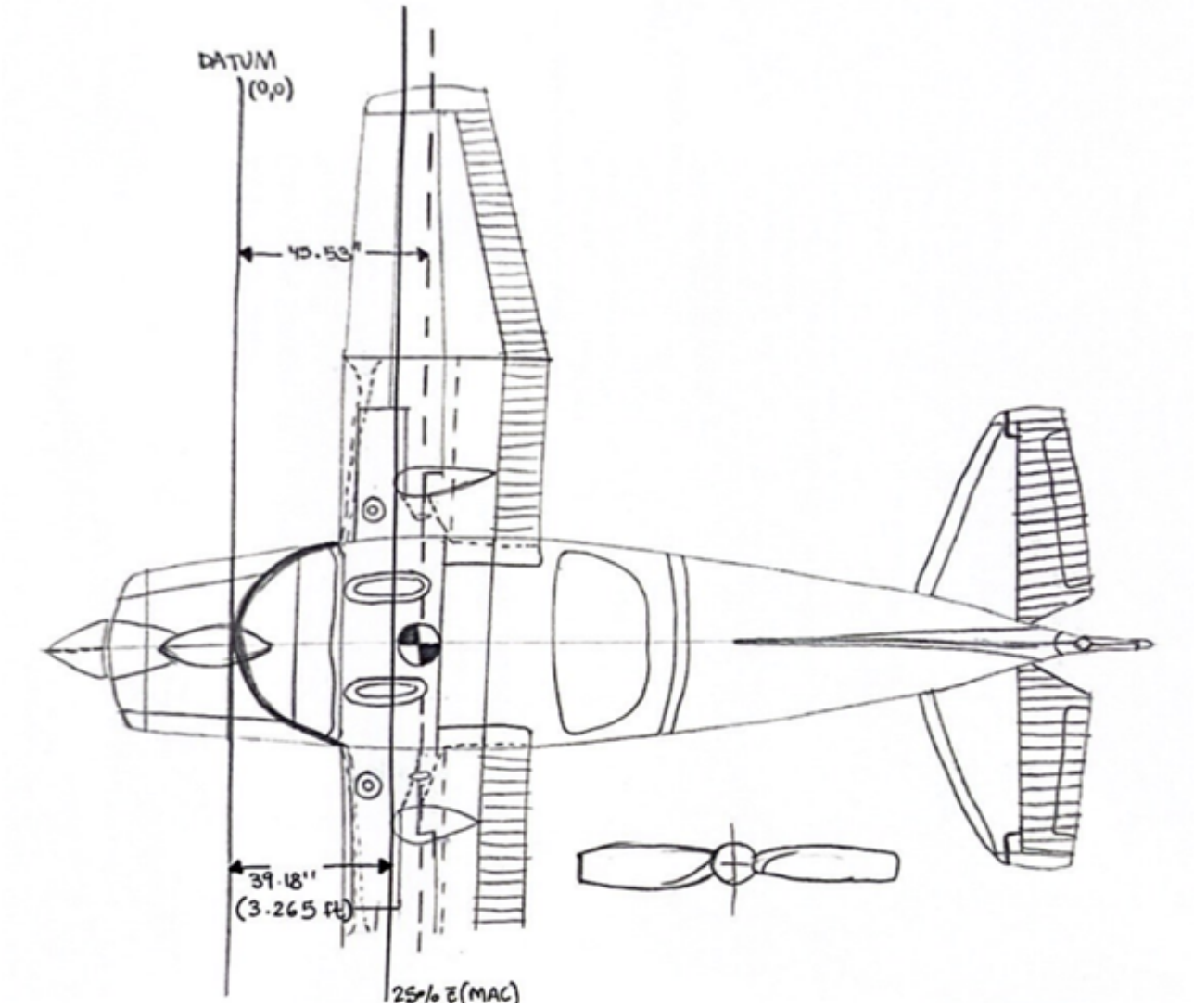

Figure 5.5: The location of 25% $\bar{c}$ with respect to the datum (39.18 inches) - Top view

5.7 Thrust Application Point

From Figure 5.4 and Figure 5.5, it can be seen that the thrust vector is parallel to the longitudinal body axis and perpendicular to the leading edge of the wing. Therefore, the unit thrust vector, in body reference frame can be expressed as:

$$\hat{T} = \begin{bmatrix} 1 \\ 0 \\ 0 \end{bmatrix} \tag{5.15}$$

The Thrust Application Point location in the aircraft with respect to the Datum is given by:

$$\mathbf{r_T} = \begin{bmatrix} \text{X:} & -32.5 \text{ in} \\ \text{Y:} & 0.0 \text{ in} \\ \text{Z:} & 0.0 \text{ in} \end{bmatrix} \tag{5.16}$$

A diagram illustrating the point of thrust application is provided in Figure 5.6.

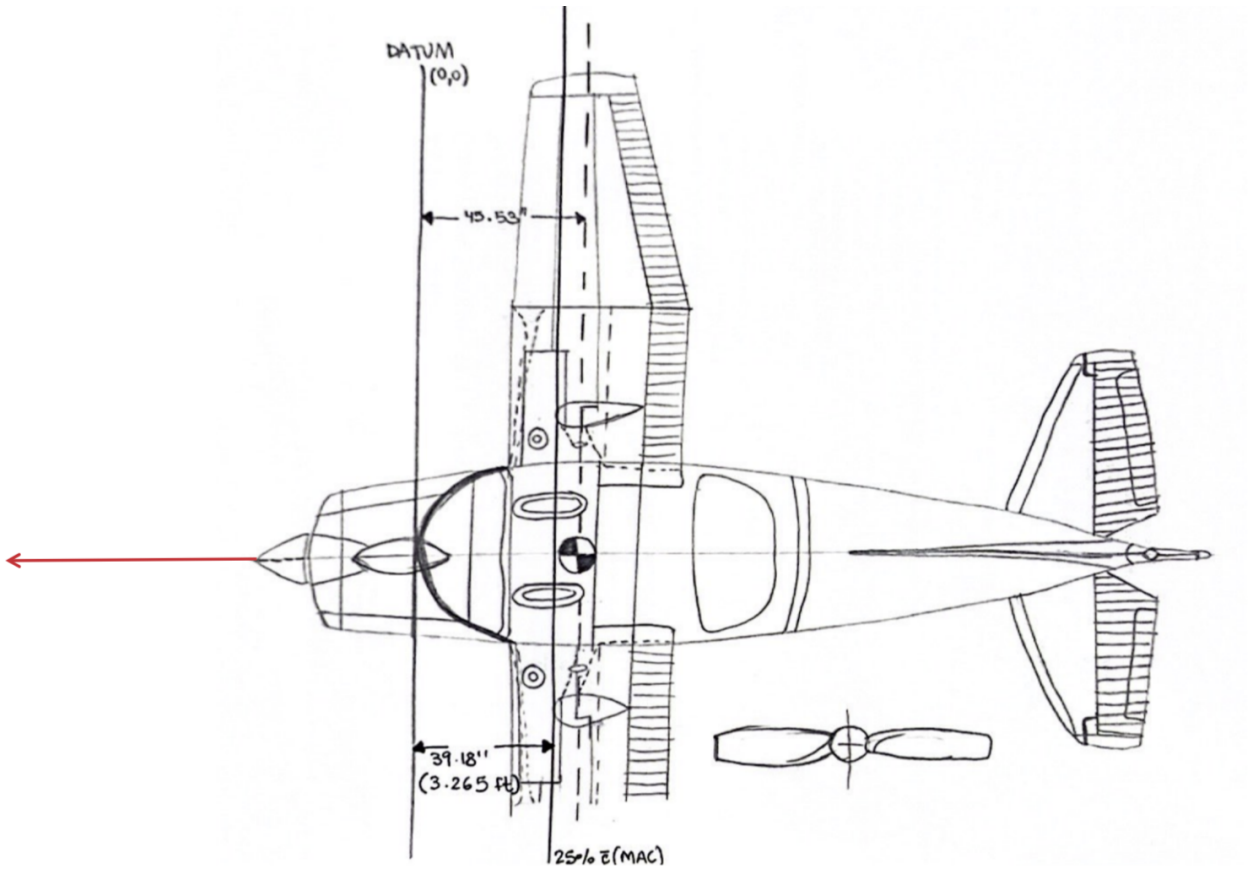

Figure 5.6: Diagram showing the thrust application point on the Cessna 182Q.

5.8 Diamond DA42 Aircraft

Although the initial modeling and simulation efforts were based on the Cessna 182Q aircraft, the project scope was adjusted mid-semester to align with the Diamond DA42 platform. To streamline the simulation effort, the DA42 was modeled as a single-engine configuration with the engine located at the centerline. This required modifying the engine thrust output to reflect equivalent performance. Specifically, a correction factor of 1.56 was applied to the Shaft Horsepower (SHP) derived from the Cessna O-470 engine model in order to match the thrust characteristics of the DA42's twin Austro AE300 engines. Details of this implementation are presented in the following chapters.

Tables 5.7 and 5.8 summarize the updated geometric properties and control surface deflections for the Diamond DA42, extracted primarily from the Type Certificate Data Sheet (TCDS) and the Pilot Operating Handbook (POH) for the Diamond DA42 [4, 5].

Table 5.7: Diamond DA42 Aircraft Geometry

Overall Dimensions	
Dimension	**Imperial**
Wingspan	44 ft
Length	28.1 ft
Height	8.2 ft
Wing Dimensions	
Wing Area	175.3 ft^2
Mean Aerodynamic Chord	4.17 ft
Aspect Ratio	11.06
Landing Gear	
Track	9.6 ft
Wheelbase	5.8 ft

Table 5.8: Control Surface Deflections for Diamond DA42

Control Surface	**Deflection Direction**	**Deflection (deg)**
Elevator	Trailing edge up	15.5°
	Trailing edge down	13°
Aileron	Trailing edge up	25°
	Trailing edge down	15°
Rudder	Left	27°
	Right	29°
Rudder (perpendicular to hinge line)	Left	18
	Right	34
Flaps	Flap setting	Down 42°
		Cruise 0°

Additional reference parameters used throughout the simulation model are summarized below:

- **MAC (Mean Aerodynamic Chord)**: 4.17 ft
- **Leading Edge of MAC from Datum**: 6.83 ft (82 inches)
- **25% MAC Location**: 6.83 ft + 0.25 × 4.17 ft = 7.87 ft
- **Center of Gravity (CG)**: 7.88 ft from datum
- **Aerodynamic Center (AC)**: 7.87 ft from datum
- **Engine Location**: 6.5 ft from datum

Chapter 6

Longitudinal Modeling

Chapter Objectives

1. **Engine and Propeller Model Concept:** Design a conceptual flowchart for the integration of the engine and propeller models.
2. **Lookup Table Development:** Generate lookup tables for Shaft Horsepower (SHP) based on the Cessna O-470 engine specs and scale them to match the DA42 engine thrust characteristics.
3. **Propeller Efficiency Integration:** Develop a MATLAB script to generate the propeller efficiency table using McCauley C76 data.
4. **Simulation and Variant Setup:** Build the complete Simulink simulation using referenced and variant subsystems for engine, aerodynamics, and atmosphere configurations.

6.1 Engine and Propeller Model

The engine modeling began with integration of a DA42-equivalent engine concept, as illustrated in Figure 6.1. The engine model was implemented in Simulink (Figure 6.2), incorporating performance data from the *O-470 Overhaul Manual* [6].

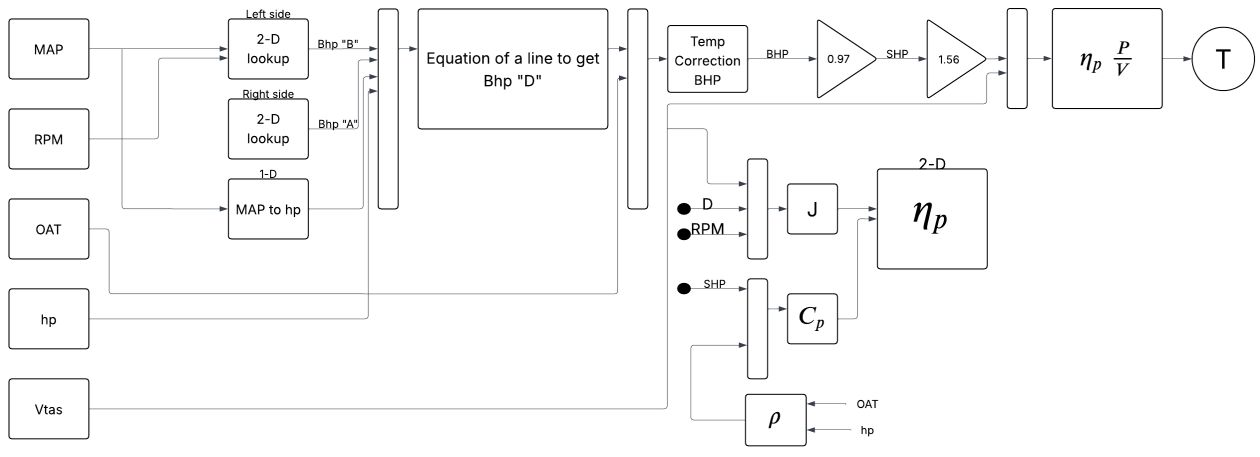

Figure 6.1: Engine and propeller integration flowchart.

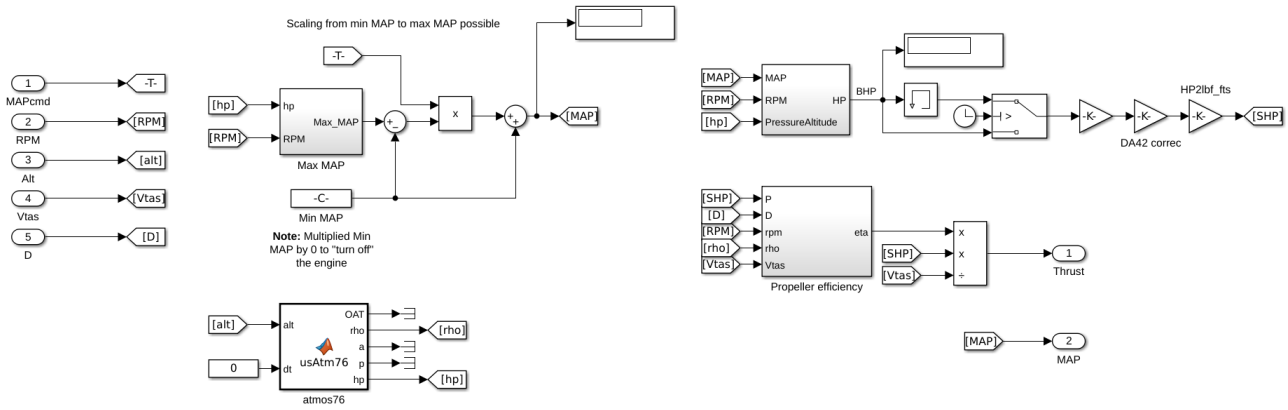

Figure 6.2: Simulink model of the engine.

6.1.1 Lookup Table Construction

Two lookup tables were derived from the engine performance charts:

- `HP_table_Ay`: Sea-level BHP from MAP (inHg) and RPM.
- `HP_table_Ax`: BHP from RPM and pressure altitude (0–20k ft).

The computed BHP is scaled by 0.97 to obtain SHP, and then multiplied by a factor of 1.56 to match the DA42 thrust output.

6.1.2 Propeller Efficiency

The propeller efficiency table was generated using the `PropellerEfficiencyTable.m` script. The McCauley C76 propeller data (PDF chart) was digitized to form a 2D lookup of η as a function of:

- Advance Ratio $J = \frac{V}{ND}$
- Power Coefficient $C_p = \frac{BHP}{\rho N^3 D^5}$

6.2 Simulation Setup

The Simulink simulation is structured using a top-level Referenced Subsystem, which represents the entire aircraft model. This approach allows the subsystem to be stored in a separate file and be reused across different applications, such as drag curve tuning and model validation, ensuring modularity and allowing an easy maintenance.

Within the aircraft subsystem, key components—such as the engine, aerodynamics, and atmosphere models are implemented as *Variant Subsystems*. This enables flexible configuration by allowing different modeling approaches or datasets to be toggled during simulation setup, depending on the specific analysis being performed.

Engine Model Variants

- **Default (1):** The original engine model used in the Navion simulation.
- **DA42 Engine (2):** A modified engine model based on the Cessna 182Q, scaled using a correction factor to approximate the combined thrust output of a twin-engine DA42.

Atmosphere Model Variants

- **Default (1):** The standard Navion atmospheric model.
- **Atmos76 (2):** A U.S. Standard Atmosphere 1976 model that computes atmospheric properties (e.g., temperature, pressure, and density) based on geometric altitude in feet.

Aerodynamics Model Variants

- **Default (1):** Aerodynamic coefficients C_L, C_D, C_m, C_Y, C_l, and C_n are defined using constant stability and control derivatives.
- **PID-Based (2):** Selected aerodynamic coefficients are defined using lookup tables obtained through parameter identification (PID) from flight data.

To run a simulation using the desired configuration, the user defines a structure named `userVariants` as shown below:

```
userVariants.Engine = 2;
userVariants.Atmosphere = 2;
userVariants.Geometry = 2;
userVariants.Stability = 2;

SimIn = simSetup(userVariants);
```

The function `simSetup` automatically selects the appropriate variant subsystems and loads the required data and parameters, preparing the simulation environment accordingly.

6.3 Aerodynamic Modeling

The aerodynamic model was developed from flight data using SIDPAC. The longitudinal coefficients identified were:

- $C_D = f(\alpha)$
- $C_L = f(\alpha)$
- $C_m = f(\alpha, q, \delta_e)$

The lateral-directional model (covered in chapter 7) includes:

- $C_Y = f(\beta)$
- $C_n = f(\beta, p, r, \delta_a)$

- $C_l = f(\beta, p, r, \delta_r)$

Each coefficient was estimated using linear regression techniques over time windows where specific excitation maneuvers were performed. The resulting coefficients were stored in MATLAB `.mat` files and integrated into Simulink as lookup tables for use in simulation.

6.3.1 Procedure Using SIDPAC

The aerodynamic model derivation followed these steps:

1. The flight data file `PID_GearUP_FlapsUP.csv` was loaded into MATLAB and the first 90 columns were extracted.
2. The `sid` command launched the SIDPAC GUI.
3. A maneuver cut was performed on the alpha (angle of attack) plot, selecting windows where the aircraft was near trim.
4. The selected maneuver data was validated and matched to expected flight conditions.
5. Linear regression was applied to estimate the aerodynamic coefficients.

For each maneuver, the angle of attack (α) at trim was computed as the average of a few samples immediately preceding the maneuver.

6.3.2 Automation and Model Formulation

To streamline the process, a MATLAB script was developed to automate the identification of aerodynamic derivatives from raw flight data. The script:

- Identifies maneuver time windows.
- Extracts corresponding data slices.
- Builds a regressor matrix for each coefficient.
- Runs a least-squares linear regression.
- Saves the results for Simulink integration.

The regression models found to be most reliable were:

- $C_D = f(\alpha) + \text{bias}$
- $C_L = f(\alpha) + \text{bias}$
- $C_m = f(\alpha, q, \delta_e) + \text{bias}$
- $C_Y = f(\beta) + \text{bias}$
- $C_n = f(\beta, p, r, \delta_a) + \text{bias}$
- $C_l = f(\beta, p, r, \delta_r) + \text{bias}$

6.3.3 Integration into Simulink

Each coefficient table was saved with the associated flight data and loaded into the aircraft model during initialization. In the case of lateral-directional coefficients, individual estimates from each maneuver were averaged to generate constant gains.

Additionally, the values for the pitch rate damping derivative (C_{mq}) and the elevator control derivative ($C_{m\delta_e}$) were computed by averaging the results across all identified maneuver windows. These constants were used in place of full lookup tables and implemented directly in the aerodynamic force models. Their values are summarized in Table 6.1.

Table 6.1: Average Values for Longitudinal Stability Derivatives

Coefficient	Value
C_{mq}	-8.9636
$C_{m\delta_e}$	-0.5371

Once the aerodynamic coefficients were identified, the resulting lookup tables were integrated into the Simulink aircraft model. Figures 6.3, 6.4, and 6.5 show the generated lookup tables for C_D, C_L, and C_m, respectively.

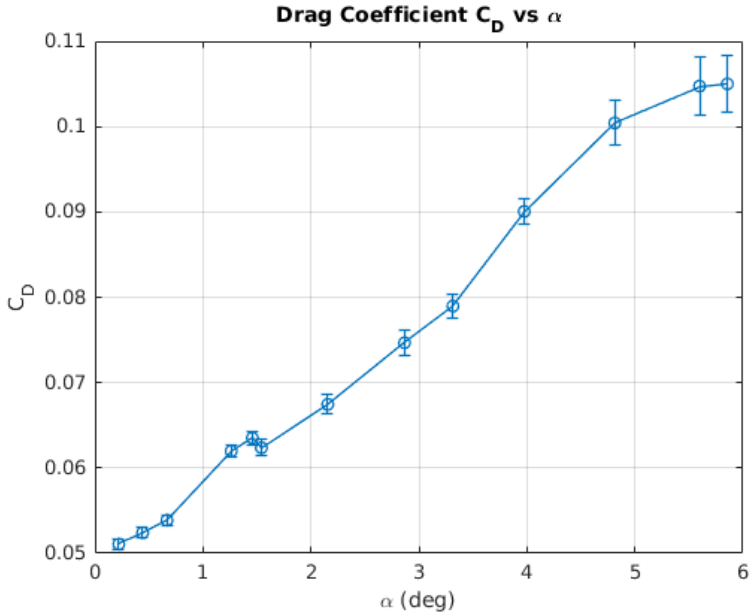

Figure 6.3: Drag coefficient C_D as a function of angle of attack α.

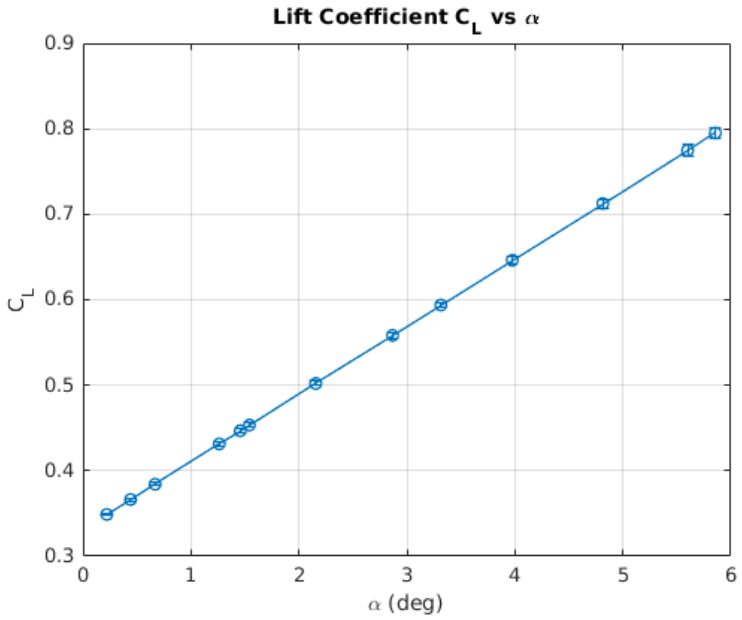

Figure 6.4: Lift coefficient C_L as a function of angle of attack α.

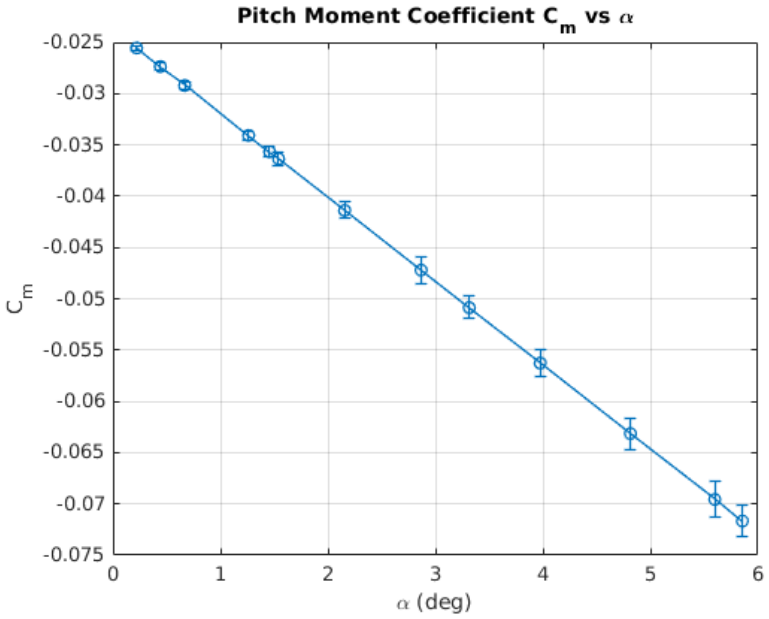

Figure 6.5: Pitching moment coefficient C_m as a function of angle of attack α.

This integration allows the Simulink model to dynamically respond to control inputs and flight conditions based on real aircraft behavior, significantly increasing simulation fidelity.

6.4 Drag Curve Tuning

To improve the fidelity of the simulation, the drag curve was refined using a method similar to parameter identification, but focused specifically on steady-state (trim) segments rather than dynamic maneuvers. With this approach captures flight conditions where aerodynamic forces and moments are balanced and predictable, unlike during transient maneuvers.

6.4.1 Trim Segment Selection and Reference Generation

Flight data was first examined to identify time intervals where the aircraft was trimmed prior to pilot-induced maneuvers. These windows provided:

- A trim state vector (attitude, velocity, etc.)
- Commanded control surface positions and engine settings, including Manifold Air Pressure (MAP)

Each operating point was replicated in the nonlinear 6-DoF Simulink model (configured with the DA42 engine variant) and trimmed using the `JJ_TRIM` algorithm. The resulting simulated MAP was plotted against measured MAP from the flight data.

Since the MAP sensor trace in the flight data was noisy, a smoothed reference curve was generated by fitting a second-order polynomial to the raw MAP measurements. This allowed comparison between simulation and both raw and smoothed references, as shown in Figure 6.6.

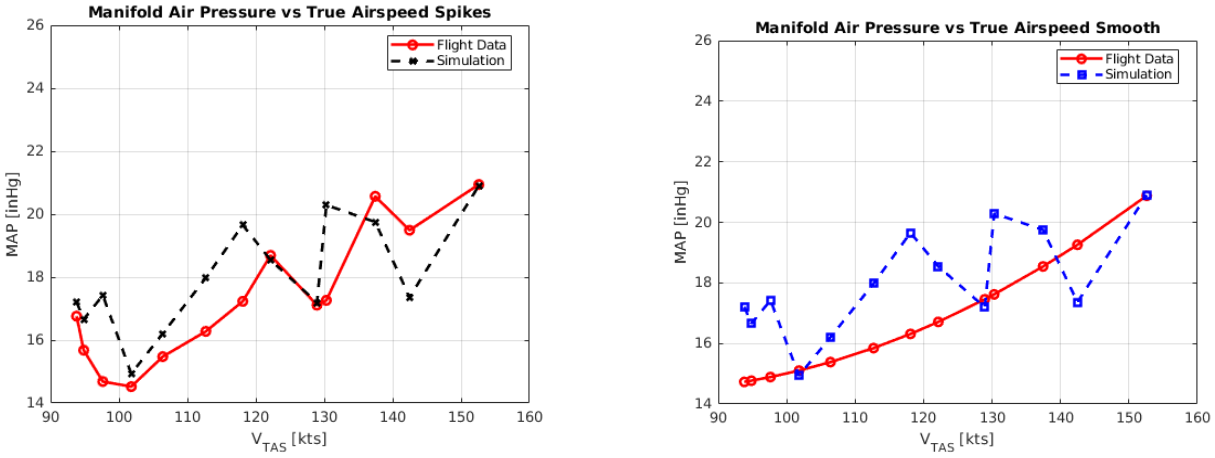

Figure 6.6: MAP comparison between raw flight data, smoothed flight data and simulation (no drag correction).

6.4.2 Iterative Correction of C_D

To minimize the differences between the simulation and the reference MAP, the drag coefficient C_D was treated as an unknown variable and solved using a bisection root-finding algorithm. For each trim case, C_D was perturbed until the simulated MAP matched the measured or smoothed reference.

This process was repeated across multiple trim conditions, generating two correction curves (as shown in Figure 6.7):

- One based on matching to noisy MAP values
- Another based on matching to smoothed MAP values

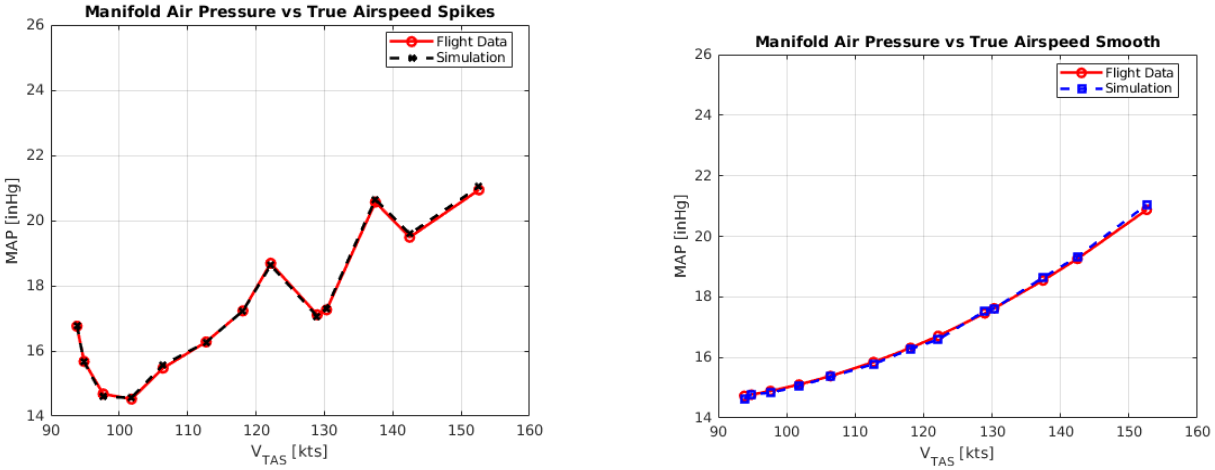

Figure 6.7: MAP comparison between raw flight data, smoothed flight data and simulation (MAP matching).

6.4.3 Final Drag Curve

To produce a final, smoothed drag curve, the following weighted average was used:

- 50% original drag curve
- 25% correction from noisy MAP
- 25% correction from smoothed MAP

The comparison of the original and corrected curves is shown in Figure 6.8, followed by the finalized drag curve in Figure 6.9.

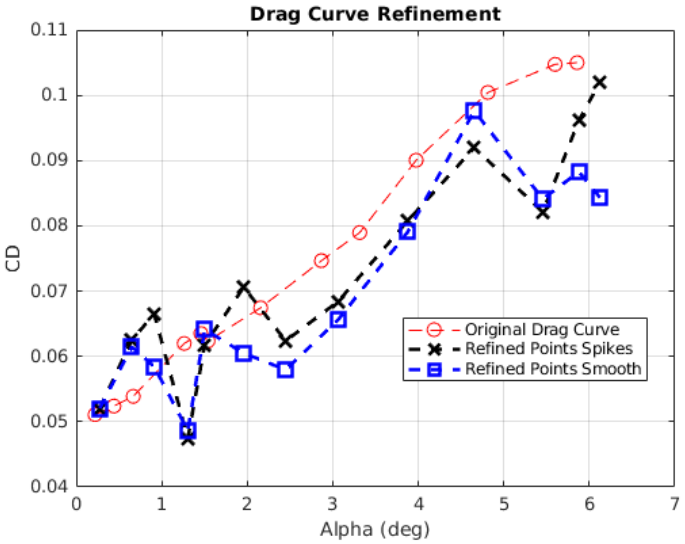

Figure 6.8: Comparison of original and corrected drag curves.

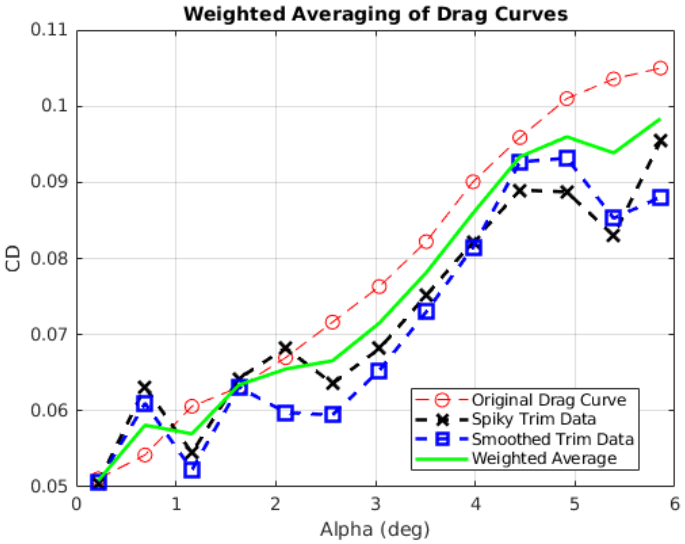

Figure 6.9: Final blended drag curve used in simulation.

To visually verify the effect of the correction, the updated drag curve was re-evaluated against the original flight data, both noisy and smoothed. As shown in Figure 6.10, the new drag curve substantially reduces the mismatch between simulation and flight data.

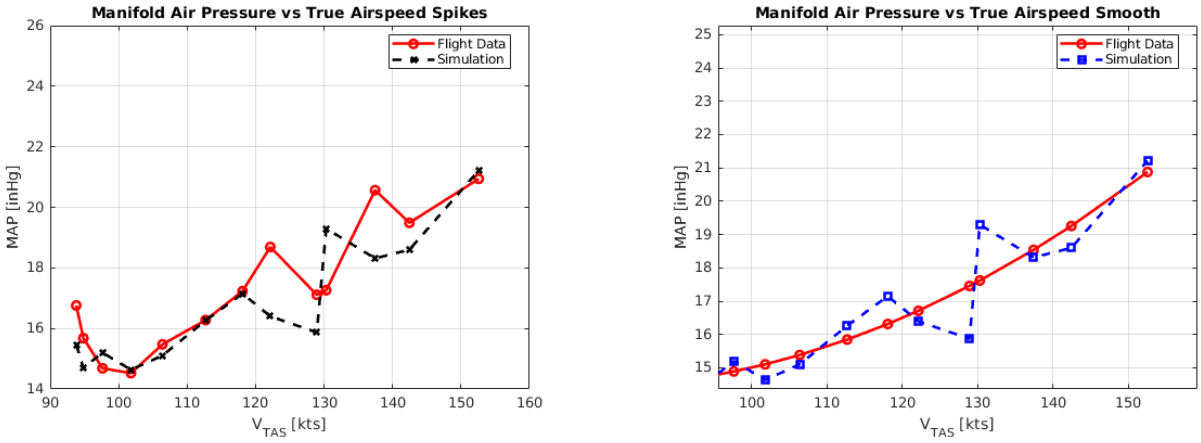

Figure 6.10: MAP comparison between raw flight data, smoothed flight data and simulation (corrected drag curve).

Chapter 7

Lateral-Directional Modeling

Chapter Objectives

1. **Estimate Lateral-Directional Stability and Control Derivatives:** Identify and extract the lateral-directional aerodynamic and control derivatives for the Gear-Up, Flaps-Up configuration using flight data. Describe the methodology used for data segmentation, regression modeling, and coefficient averaging.

The lateral-directional aerodynamic model builds upon the methodology described in chapter 6. The same process was followed for each relevant coefficient: loading trimmed maneuver windows, performing linear regression, and saving the resulting coefficients into MATLAB `.mat` files.

The following coefficients were estimated as the average of multiple values across the different flight maneuvers, and were implemented as constants within the simulation:

Table 7.1: Average Values for Lateral-Directional Stability and Control Derivatives

Coefficient	**Value**
$C_{Y\beta}$	-0.2778
$C_{L\beta}$	-0.1413
C_{L_p}	-0.6850
C_{L_r}	0.2781
$C_{L_{\delta a}}$	-0.1778
$C_{N\beta}$	0.0491
C_{N_p}	-0.1357
C_{N_r}	-0.0817
$C_{N_{\delta r}}$	0.0688

7.1 Bias Correction

During implementation, it was observed that the lateral-directional model produced an unintended roll and yaw even in the absence of pilot input. After a thorough analysis, this behavior was attributed to non-zero bias terms in the linear regression models for C_l and C_n, which at the same time reflects slight asymmetries in the DA42's geometry. To eliminate this effect and ensure neutral behavior in steady-state flight, the constant bias terms in the C_l and C_n models were manually set to zero. This correction allowed the aircraft to maintain level and coordinated flight without input, improving the fidelity and usability of the simulation model.

Chapter 8

Static Derivatives

Chapter Objectives

1. **Drag Curve vs. Angle of Attack:** Determine the drag coefficient as a function of angle of attack for the Gear-Up, Flaps-Up configuration using both regression modeling and flight data approximations.

2. **Lift Curve vs. Angle of Attack:** Estimate the lift coefficient as a function of angle of attack and validate the assumptions under steady flight conditions.

3. **Pitching Moment Curve vs. Angle of Attack:** Estimate the pitching moment coefficient as a function of angle of attack and validate the assumptions under steady flight conditions.

This chapter focuses on computing the static longitudinal derivatives $C_{D\alpha}$, $C_{L\alpha}$ and $C_{m\alpha}$ from trimmed flight conditions, where the aircraft maintains a steady speed and angle of attack. Under these conditions, the net acceleration is near zero, therefore we can approximate the aerodynamic forces from flight data as follows:

$$T \approx D \quad \text{and} \quad L \approx W$$

These assumptions are used to derive simplified formulas for estimating the drag and lift coefficients based on measurements of the thrust, dynamic pressure, and aircraft weight.

8.1 Drag coefficient approximation

In order to approximate the drag coefficient C_D from flight data, we assume that under trim conditions the total engine thrust T equals the total drag force D:

$$T \approx D = C_D \cdot \bar{q} \cdot S$$

Solving for C_D, we obtain the approximation:

$$C_D \approx \frac{T}{\bar{q} \cdot S}$$

Here, $\bar{q}$ is the dynamic pressure, and S is the reference wing surface area. Both $\bar{q}$ and S are obtained from flight data, and T is computed as the sum of thrust from both engines. This approximation is evaluated over selected time intervals where the aircraft is assumed to be in steady flight. For each interval, the average thrust, dynamic pressure, and surface area are used to compute a C_D value. In Figure 8.1, we compare the drag coefficient values obtained from three sources:

1. Flight data measurements of C_D
2. The regression model obtained in chapter 6.
3. The approximation derived from thrust and dynamic pressure

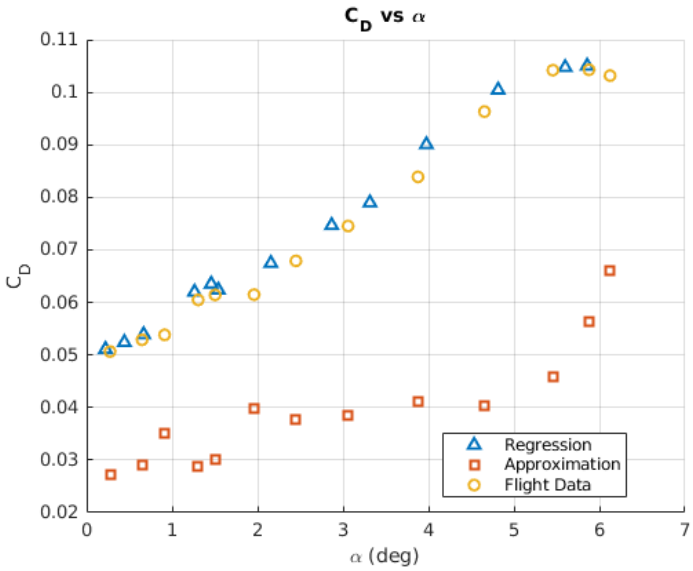

Figure 8.1: Comparison of C_D from flight data, regression model, and approximation as a function of angle of attack.

As we can see from Figure 8.1, there is a noticeable difference between the approximation and the other two methods. On one side, the flight data and the regression curve match closely, which indicates that the regression is a good model. However, the approximation appears to underestimate the drag coefficient across all angles of attack. If the actual drag coefficient is greater than the approximation, the difference suggests that:

$$D > T \Rightarrow T = D - X$$

Where X is a force that is not captured possibly due to measurement inaccuracies in thrust or unaccounted aerodynamic effects.

8.2 Lift coefficient approximation

A similar approach is applied to approximate the lift coefficient C_L, leveraging the assumption that the aircraft is maintaining level flight during the selected intervals. In these cases, the total lift force L is approximately equal to the aircraft weight W:

$$L \approx W = C_L \cdot \bar{q} \cdot S$$

Solving for C_L:

$$C_L \approx \frac{W}{\bar{q} \cdot S}$$

The weight W is computed using the aircraft mass (from flight data) multiplied by the gravitational constant $g = 32.174$ ft/s^2. Figure 8.2 shows a comparison of the lift coefficient values from:

1. Flight data measurements of C_L
2. The regression model obtained in chapter 6.
3. The approximation derived from weight and dynamic pressure

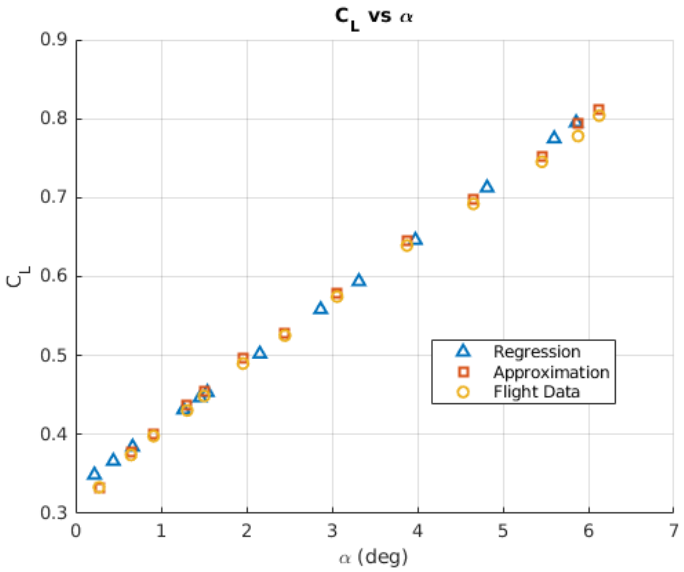

Figure 8.2: Comparison of C_L from flight data, regression model, and approximation as a function of angle of attack.

As shown in Figure 8.2, the approximation method closely matches both the regression model and the measured flight data. This validates the assumption that lift equals weight in steady, level flight.

8.3 Pitching moment coefficient approximation

To approximate the pitching moment coefficient C_m from flight data, we consider the trimmed steady-flight condition, where the net pitching moment is approximately zero. The general expression for the pitching moment coefficient is given by:

$$C_m = C_{m_\alpha} \cdot \alpha + C_{m_{\delta_e}} \cdot \delta_e + C_{m_q} \cdot q + C_{mo}$$

In steady, trimmed flight, we assume the pitch rate $q \approx 0$ and $C_m \approx 0$. Therefore, the equation simplifies to:

$$C_{m_\alpha} \cdot \alpha + C_{m_{\delta_e}} \cdot \delta_e + \text{bias} \approx 0$$

Rearranging the terms, we isolate the contribution of the elevator deflection:

$$C_m(\alpha) \approx -C_{m_{\delta_e}} \cdot \delta_e$$

In this approximation, δ_e (elevator deflection) is obtained directly from the flight data. The coefficient $C_{m_{\delta_e}}$ is extracted from the linear regression model obtained for each flight segment. Figure 8.3 presents a comparison between the regression model and the approximation based on elevator deflection.

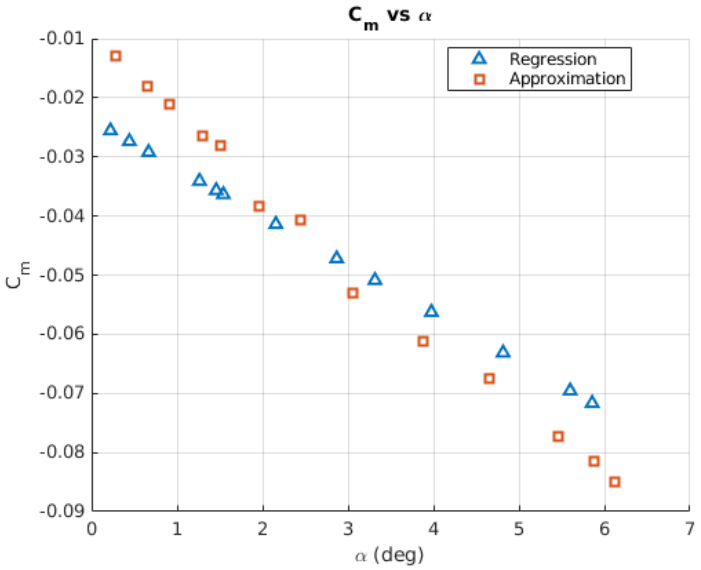

Figure 8.3: Comparison of C_m from regression model and approximation as a function of angle of attack.

Chapter 9

Validation

Chapter Objectives

1. **Understanding Validation Criteria under 14 CFR Part 60:** Introduce the regulatory framework for Flight Simulation Training Devices (FSTDs), and identify the three specific validation criteria implemented in this study based on FAA Level 6 FTD standards.

2. **Defining Tolerance Envelopes:** Present the tolerance bands used in model validation.

3. **Evaluating and Refining Model Derivatives:** Discuss the sensitivity of key aerodynamic derivatives on the validation metrics. Detail the tuning actions that were implemented to bring the model into compliance with validation standards.

For the validation, Federal Aviation Administration FAA 14 CFR Part 60[7] standards are followed. Although there are over 100 validation test criteria defined, this project focuses on three required tests to meet the Level 6 Flight Test Device (FTD) standard. These include one short-period validation for the longitudinal model and one Dutch roll validation for the lateral-directional model.

The longitudinal model is validated using plots for N_z, q, and α, while the lateral-directional model is validated using β, p, and r. The simulation outputs are compared against flight test data, and results must remain within the tolerances listed in Table 9.1.

Table 9.1: Model Output Tolerances

Longitudinal model		
N_z	± 0.1	g
q	± 2	deg/s
α	± 1.5	deg
Lateral model		
β	± 1.5	deg
p	± 2	deg/s
r	± 2	deg/s

Figures 9.1, 9.2, and 9.3 show the results for the longitudinal model. The red lines represent the tolerance envelope, while the blue lines show the simulation results. The longitudinal model stayed well within all validation bounds and did not require any adjustments.

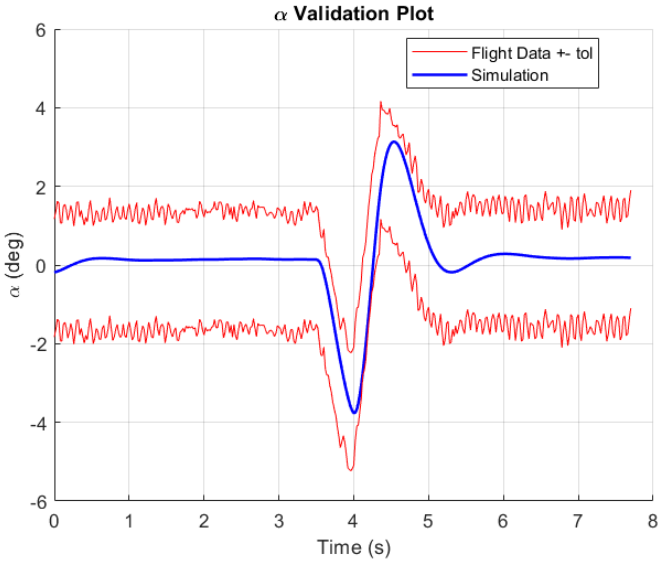

Figure 9.1: Validation result for angle of attack (α).

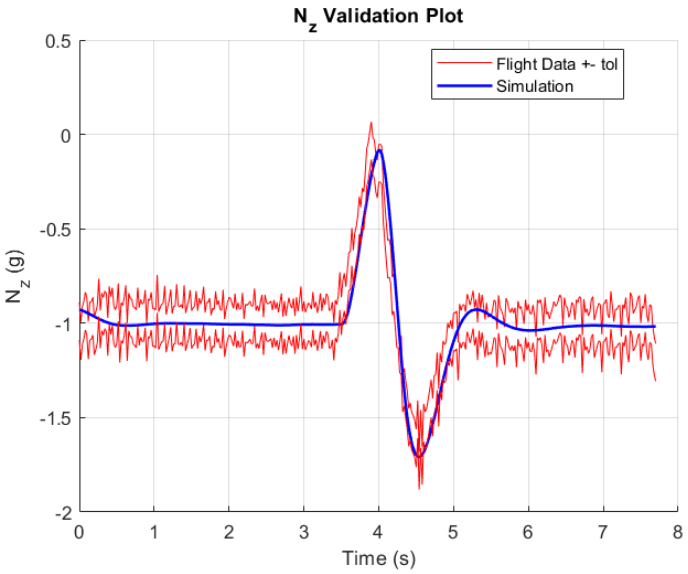

Figure 9.2: Validation result for vertical acceleration (N_z).

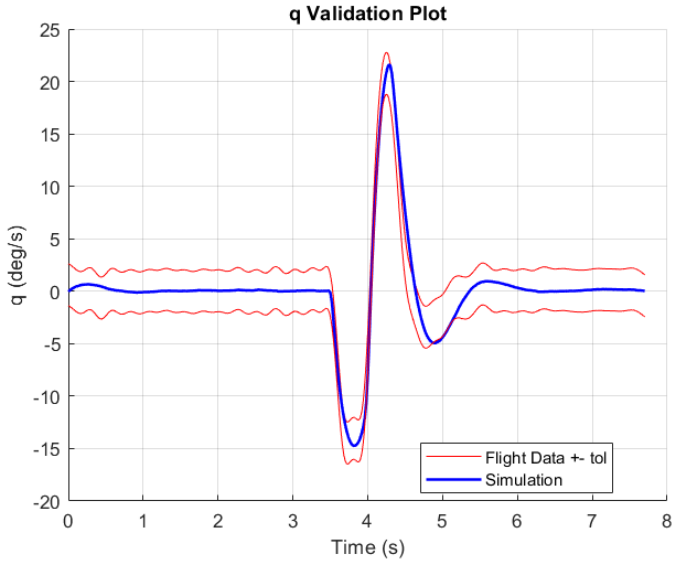

Figure 9.3: Validation result for pitch rate (q).

Table 9.2: Longitudinal Model: Control Input Biases and Time Within Tolerance

Control Input Biases	
Elevator Bias	$-0.20°$
Aileron Bias	$-0.11°$
Rudder Bias	$+2.08°$
Throttle Bias	0.134 (normalized)
Percentage of Time Within Tolerance	
α tolerance $\pm 1.5°$	100.0%
q tolerance $\pm 2.0°/s$	92.5%
N_z tolerance ± 0.10 g	83.7%

The lateral-directional validation results are shown in Figures 9.4, 9.5, and 9.6. Initially, the simulation outputs deviated slightly from the tolerance bands. To improve fidelity, specific derivatives had to be tuned, which required an analysis of the aerodynamic derivatives effects.

Increasing $C_{L\beta}$ improved lateral stability, resulting in stronger roll rates, reduced yaw rates, and faster response in sideslip. Increasing C_{Lp} had the opposite effect: it reduced roll rate, increased yaw rate, and delayed sideslip. Adjustments to C_{Lr} reduced the overall magnitude of lateral response due to its coupling effect. Likewise, increasing $C_{L\delta a}$ exaggerated all outputs.

For yawing moment behavior, increasing $C_{N\beta}$ (weathervane stability) and C_{Nr} (yaw damping) helped reduce oscillations across all outputs. These coefficients govern how the aircraft naturally aligns to the relative wind and resist prolonged yaw, which indirectly stabilizes roll and sideslip as well.

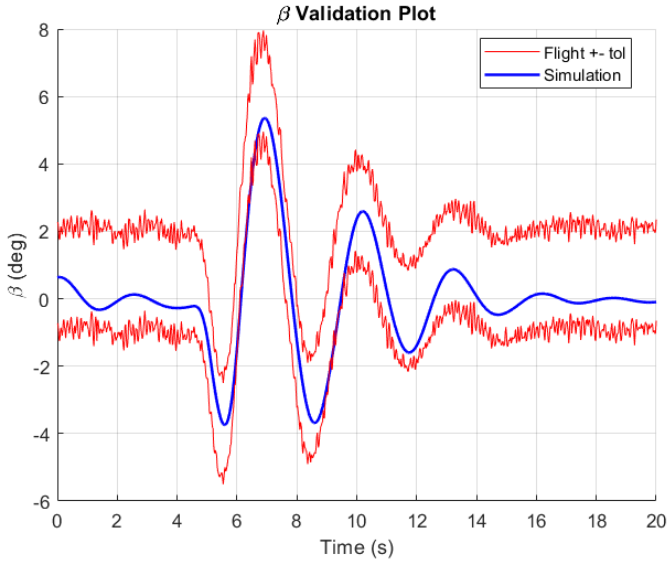

Figure 9.4: Validation result for sideslip angle (β).

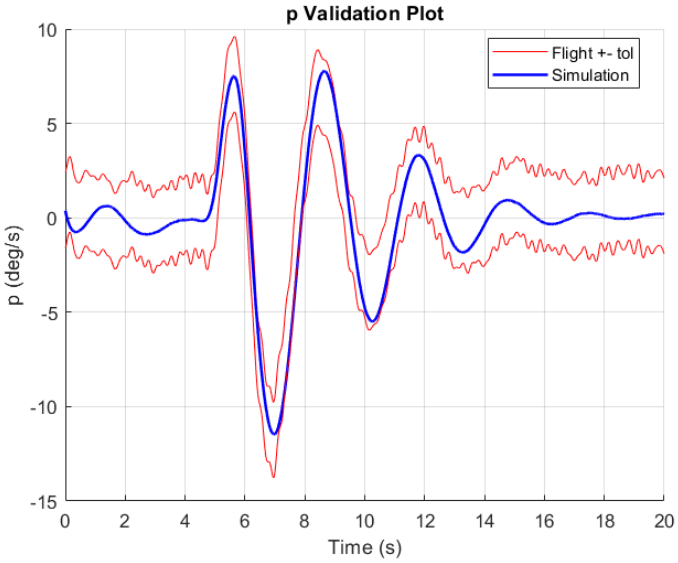

Figure 9.5: Validation result for roll rate (p).

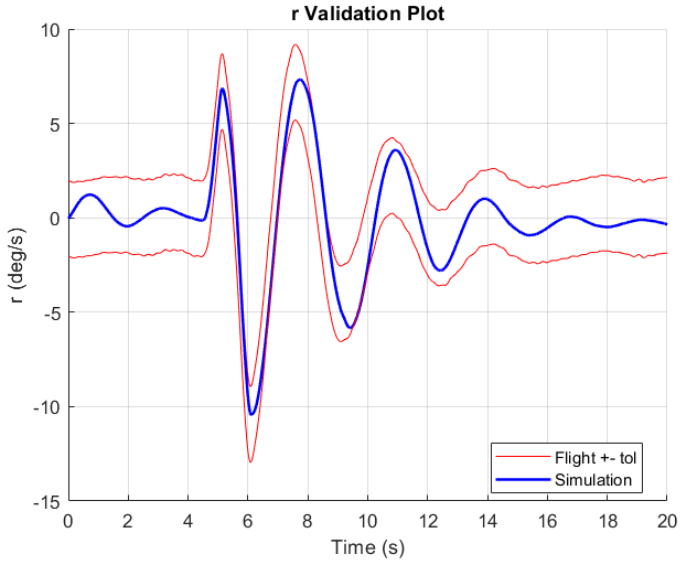

Figure 9.6: Validation result for yaw rate (r).

Table 9.3: Lateral Model: Control Input Biases and Time Within Tolerance

Control Input Biases	
Elevator Bias	$-0.97°$
Aileron Bias	$+0.05°$
Rudder Bias	$+3.03°$
Throttle Bias	0.010 (normalized)
Percentage of Time Within Tolerance	
β tolerance $\pm 1.5°$	96.5%
p tolerance $\pm 2.0°/s$	99.0%
r tolerance $\pm 2.0°/s$	98.5%

9.1 Final Modifications

While the longitudinal model remained unaltered during validation, some refinements were performed to the lateral-directional model. Specifically:

- C_{Np} (roll rate influence on yawing moment) was scaled by a factor of 1.5.
- $C_{N\delta r}$ (yaw control power) was scaled by a factor of 1.2.

These changes brought the simulation results for β, p, and r within the FAA-defined tolerance bands, aligning the results with flight data.

Additionally, minor control input biases were observed. In particular, elevator and throttle commands showed slight steady-state offsets compared to the flight test data. To address this:

- The lower bound for Manifold Air Pressure (MAP) in the engine model's lookup table was adjusted to 17 inHg.

- A bias of 0.02 radians was added to the x-values of the C_m (pitch moment) curve. This correction aligned the elevator command behavior with observed flight data.

These corrections—though small—played a crucial role in achieving full compliance with the validation tolerances, ensuring that both the aerodynamic forces and required control inputs closely match actual flight test behavior.

Bibliography

[1] T. Berger, M. Tischler, S. G. Hagerott, D. Gangsaas, and N. Saeed, *Lateral/Directional Control Law Design and Handling Qualities Optimization for a Business Jet Flight Control System*, 2013. [Online]. Available: https://arc.aiaa.org/doi/abs/10.2514/6.2013-4506

[2] T. Lombaerts, J. Kaneshige, S. Schuet, G. Hardy, B. L. Aponso, and K. H. Shish, *Nonlinear Dynamic Inversion Based Attitude Control for a hovering quad tiltrotor eVTOL vehicle*, 2019. [Online]. Available: https://arc.aiaa.org/doi/abs/10.2514/6.2019-0134

[3] Cessna Aircraft Company, *Pilot's Operating Handbook: Cessna Model 182Q*, http://kirtlandflightcenter.org/wp-content/uploads/C182-POH-w-bookmarks.pdf, 1978.

[4] European Aviation Safety Agency (EASA), *Type Certificate Data Sheet for EASA.A.005 – Diamond DA 42 and Variants*, 2013. [Online]. Available: https://www.easa.europa.eu/sites/default/files/dfu/certification-type-certificates-docs-aircraft-EASA-TCDS-A.005_Diamond_DA_42_and_variant-22-14062013.pdf

[5] Diamond Aircraft Industries GmbH, *Airplane Flight Manual DA42 Twin Star*, 2004. [Online]. Available: http://support.diamond-air.at/fileadmin/uploads/files/after_sales_support/DA42_Twin_Star/Airplane_Flight_Manual/Basic_Manual/70105e-Rev9-complete.pdf

[6] Teledyne Industries, Inc., *O-470 Series Aircraft Engines Overhaul Manual*, https://www.xuefeiji.org/public/uploads/files/20211019/1_20211019151321e4774.pdf, October 1992.

[7] Federal Aviation Administration, "14 CFR Part 60 (2016) NSP Consolidated Version," https://www.faa.gov/sites/faa.gov/files/about/initiatives/nsp/14CFR60_Searchable_Version.pdf, 2016.

Appendix A

Extra Credit - Anupama Kar

A MATLAB script was created to analyze the aerodynamic data across different angles of attack (α) by processing 11 datasets (`fdata1.mat` to `fdata11.mat`). These `fdata.mat` files are obtained by doing maneuver cuts around the 11 clearly visible maneuvers on SIDPAC. It first computes the mean of the first 50 values from the 4th column of each file, storing them in `alphainterest`, which serves as the x-axis for all plots. Then, for each dataset, it applies bias corrections and combines error estimates using the `hypot` function to calculate final aerodynamic coefficients: $C_{M\alpha}$, $C_{M\bar{q}}$, $C_{M\delta e}$, C_L, and C_D, along with their respective errors. Linear or quadratic regression is performed for each coefficient against α to identify trends. Finally, the script creates a figure with five subplots, each displaying one coefficient with error bars and its regression line, giving insight into how each aerodynamic parameter varies with angle of attack.

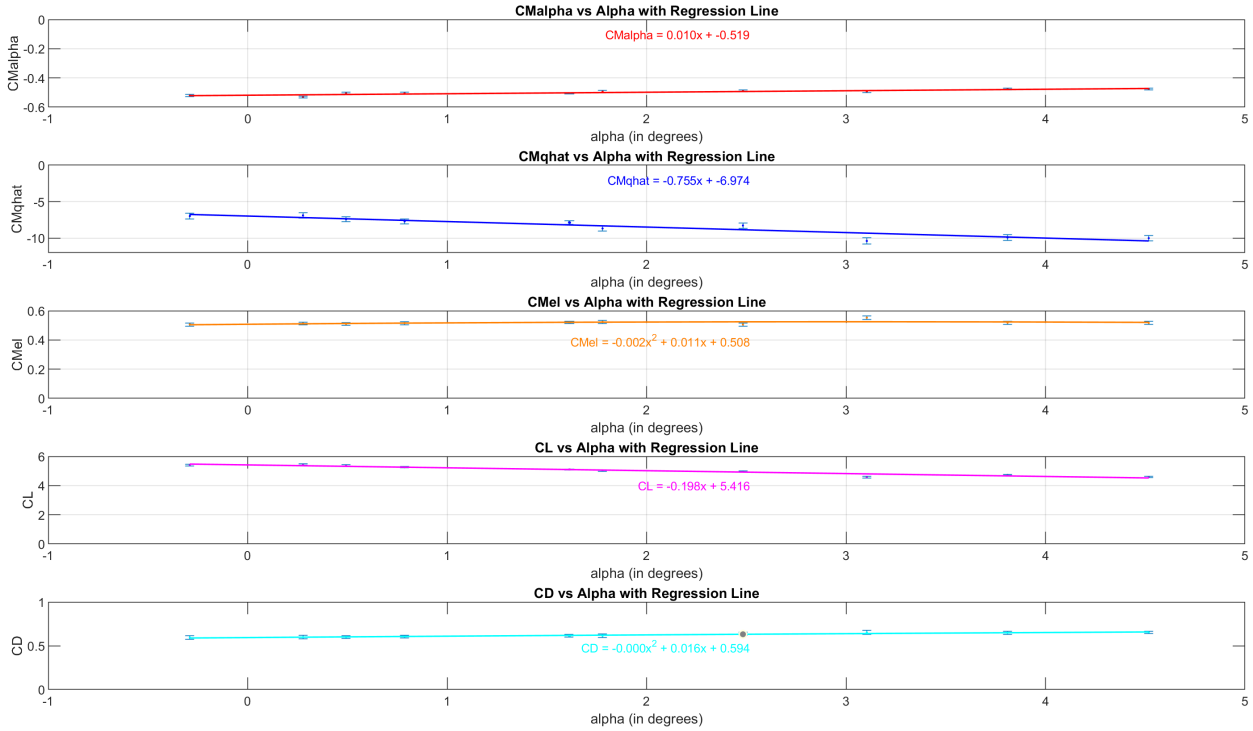

Figure A.1: Function for each derivative vs. α